REPORT DOCUMENTATION PAGE

Form Approved
OMB No. 0704-0188

1. AGENCY USE ONLY (Leave blank)	2. REPORT DATE	3. REPORT TYPE AND DATES COVERED
	October 31, 1995	Final Technical Report 04/93 - 08/95

4. TITLE AND SUBTITLE
Hybrid Ceramic Matrix Composites: A Study of Transverse Properties and Failure Modes

5. FUNDING NUMBERS
F49620-93-1-0223

6. AUTHOR(S)
L. R. Dharani and D. R. Carroll

7. PERFORMING ORGANIZATION NAME(S) AND ADDRESS(ES)
The University of Missouri-Rolla
Dept. of Mechanical & Aerospace Engineering and Engineering Mechanics
Rolla, MO 65409-0050

8. PERFORMING ORGANIZATION REPORT NUMBER
AFOSR-TR-95
0775

9. SPONSORING/MONITORING AGENCY NAME(S) AND ADDRESS(ES)
AFOSR/NA
Dr. Walter F. Jones, Program Manager
110 Duncan Avenue, Suite B115
Bolling AFB, DC 20332-0001

11. SUPPLEMENTARY NOTES

12a. DISTRIBUTION/AVAILABILITY STATEMENT
Unlimited

12b. DISTRIBUTION CODE

13. ABSTRACT (Maximum 200 words)

The purpose of this study was to demonstrate the effects, and ultimately, the advantages of forming a hybrid ceramic matrix composite (HCMC) by adding whiskers to a fiber reinforced ceramic matrix composite (FCMC). The addition of whiskers to a continuous fiber ceramic composite has been shown to produce a hybrid composite that: (1) is more stiffer, (2) resists microcracking until higher loading levels, (3) has improved transverse strength and stiffness and (4) shows improved damage tolerance when compared with fiber reinforced composites (FCMC). The modulus was found to be, on average, 212 ± 24 GPa for the hybrid system compared to 170 ± 20 GPa for the FCMC system. The ultimate strength was basically preserved, but the stress at which microcracking was first observed was increased for the hybrid system to 121.4 ± 19.0, an increase almost threefold over the FCMC system. The transverse microcracking stress was 31.0 ± 7.0 MPa for the HCMC compared with 16.4 ± 1.0 MPa for the FCMC. The ultimate strengths were 62.4 ± 7.0 MPa and 24.2 ± 6.0 MPa, respectively. The study has indeed demonstrated the benefits from hybridization of ceramic composites and provide a basis for further study.

14. SUBJECT TERMS	15. NUMBER OF PAGES
Hybrid Ceramic Matrix Composites, Microcracking, Transverse Strength, Transverse Modulus, Fabrication	105
	16. PRICE CODE

17. SECURITY CLASSIFICATION OF REPORT	18. SECURITY CLASSIFICATION OF THIS PAGE	19. SECURITY CLASSIFICATION OF ABSTRACT	20. LIMITATION OF ABSTRACT
Unclassified	Unclassified	Unclassified	UL

NSN 7540-01-280-5500

Standard Form 298 (Rev. 2-89)
Prescribed by ANSI Std. 239-18
298-102

GENERAL INSTRUCTIONS FOR COMPLETING SF 298

The Report Documentation Page (RDP) is used in announcing and cataloging reports. It is important that this information be consistent with the rest of the report, particularly the cover and title page. Instructions for filling in each block of the form follow. It is important to ***stay within the lines*** to meet ***optical scanning requirements.***

Block 1. Agency Use Only *(Leave blank)*.

Block 2. Report Date. Full publication date including day, month, and year, if available (e.g. 1 Jan 88). Must cite at least the year.

Block 3. Type of Report and Dates Covered. State whether report is interim, final, etc. If applicable, enter inclusive report dates (e.g. 10 Jun 87 - 30 Jun 88).

Block 4. Title and Subtitle. A title is taken from the part of the report that provides the most meaningful and complete information. When a report is prepared in more than one volume, repeat the primary title, add volume number, and include subtitle for the specific volume. On classified documents enter the title classification in parentheses.

Block 5. Funding Numbers. To include contract and grant numbers; may include program element number(s), project number(s), task number(s), and work unit number(s). Use the following labels:

C	- Contract	PR	- Project
G	- Grant	TA	- Task
PE	- Program Element	WU	- Work Unit Accession No.

Block 6. Author(s). Name(s) of person(s) responsible for writing the report, performing the research, or credited with the content of the report. If editor or compiler, this should follow the name(s).

Block 7. Performing Organization Name(s) and Address(es). Self-explanatory.

Block 8. Performing Organization Report Number. Enter the unique alphanumeric report number(s) assigned by the organization performing the report.

Block 9. Sponsoring/Monitoring Agency Name(s) and Address(es). Self-explanatory.

Block 10. Sponsoring/Monitoring Agency Report Number. *(If known)*

Block 11. Supplementary Notes. Enter information not included elsewhere such as: Prepared in cooperation with...; Trans. of...; To be published in.... When a report is revised, include a statement whether the new report supersedes or supplements the older report.

Block 12a. Distribution/Availability Statement. Denotes public availability or limitations. Cite any availability to the public. Enter additional limitations or special markings in all capitals (e.g. NOFORN, REL, ITAR).

DOD	- See DoDD 5230.24, "Distribution Statements on Technical Documents."
DOE	- See authorities.
NASA	- See Handbook NHB 2200.2.
NTIS	- Leave blank.

Block 12b. Distribution Code.

DOD	- Leave blank.
DOE	- Enter DOE distribution categories from the Standard Distribution for Unclassified Scientific and Technical Reports.
NASA	- Leave blank.
NTIS	- Leave blank.

Block 13. Abstract. Include a brief *(Maximum 200 words)* factual summary of the most significant information contained in the report.

Block 14. Subject Terms. Keywords or phrases identifying major subjects in the report.

Block 15. Number of Pages. Enter the total number of pages.

Block 16. Price Code. Enter appropriate price code *(NTIS only)*.

Blocks 17. - 19. Security Classifications. Self-explanatory. Enter U.S. Security Classification in accordance with U.S. Security Regulations (i.e., UNCLASSIFIED). If form contains classified information, stamp classification on the top and bottom of the page.

Block 20. Limitation of Abstract. This block must be completed to assign a limitation to the abstract. Enter either UL (unlimited) or SAR (same as report) An entry in this block is necessary if the abstract is to be limited. If blank, the abstract is assumed to be unlimited.

DISCLAIMER NOTICE

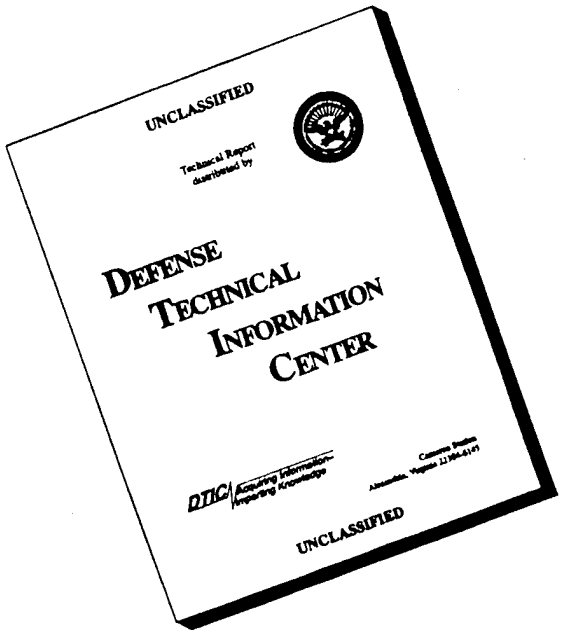

THIS DOCUMENT IS BEST QUALITY AVAILABLE. THE COPY FURNISHED TO DTIC CONTAINED A SIGNIFICANT NUMBER OF PAGES WHICH DO NOT REPRODUCE LEGIBLY.

EXECUTIVE SUMMARY

The objective of the project is to study the effects of reinforcing a ceramic matrix by aligned continuous fibers and finely dispersed whiskers on microcracking stress and transverse properties. The project duration was April 1, 1993-August 31, 1995. The work resulted in two Masters degree theses which form the final report and are attached as Appenices A and B.

Accomplishments

Fabrication of Composites: Three types of ceramic matrix composites have been fabricated. These are (i) whisker reinforced ceramic matrix composites (WCMC), (ii) continuous fiber reinforced ceramic matrix composites (FCMC), and (iii) whisker and continuous fiber reinforced hybrid ceramic matrix composites (HCMC). First FCMC and HCMC were fabricated using the conventional filament winding technique. Measured densities were close to the corresponding theoretical values, however, some difficulties were encountered in getting a uniform dispersion of whiskers in the presence of continuous fibers and the hybrid composites showed no improvement over those containing only continuous fiber composites. Therefore, the composites were fabricated by a tape casting technique and the results have been very good. In the tape casting method, volume fractions are consistent and are more accurately adjustable. Initial voids were smaller leading to lower porosity in the final product. The initial step was to produce the ceramic tape. For the whisker reinforcement, whiskers were mixed into the slurry from which the tape is cast. When making pure matrix or whisker reinforced ceramic materials the green tape was cut, stacked to the desired thickness and lamination pressed. For continuous fiber reinforcement, the fibers were first embedded into the tape in an intermediate lamination process. The final stage was to fire and heat treat the green ceramic. The tape casting technique developed during this grant period for fabricating hybrid and continuous fiber ceramic composites, has been very successful. The densities of the matrix, composites fabricated by tape casting processes were very close to the corresponding theoretical values.

Mechanical Properties: Mechanical testing (three-point bend) has been performed on an MTS 810 load frame. A metallurgical microscope was used in conjunction with the acoustic emissions equipment to verify the nature of events that occurred during testing. Post failure analysis has been performed using a scanning electron microscope. The axial microcracking stresses for the whisker reinforced ceramic matrix composites (WCMC), FCMC and HCMC, refer to the point at which the matrix material first exhibits cracks. In the HCMC system, the stress at which the matrix cracking

initiates is considerably higher than those of the other two composite systems. This is likely due to the synergism of the whiskers and the fibers acting together in the material. The transverse modulus of FCMC is significantly lower than that of either the WCMC or the neat matrix while the transverse modulus for the HCMC is somewhat closer to that of the WCMC. This trend is indicative of a relatively stronger fiber/matrix interface in the HCMC compared to the FCMC.

Failure Modes: In order to deduce the contribution of the individual constituents to the damage tolerance of the hybrid composite, the results of reinforcing the base ceramic with whiskers alone and with fibers alone was investigated. The microcracking stress for the HCMC system was consistently about 32% of the ultimate strength. The corresponding stresses for WCMC and FCMC systems were 22% and 12%, respectively. The acoustic emissions detected from the loading of the hybrid composite specimens corresponded well with the amplitudes noted from the testing of the WCMC and FCMC systems. From the stress-strain plots of the HCMC system, it is observed that not only is the onset of microcracking delayed, but the net cracking in the material before it reaches its ultimate strength is smaller than that of the FCMC. The toughening effect of the whiskers in the matrix can also be seen from examination of the transverse hybrid specimens. An examination of the path of the major crack shows that in FCMC the crack grows by connecting adjoining fibers with extensive interface debonding while in HCMC the crack tends to travel mostly in the matrix; further evidence of a stronger fiber/matrix interface. The axial specimens show that the extent of fiber pull-out for the HCMC is not as pronounced as the FCMC. The whiskers in HCMC in spite of being randomly oriented, show significant (whisker) pull-out thus adding to the toughening.

Conclusions: The purpose of this study was to demonstrate the effects, and ultimately, the advantages of forming a hybrid ceramic composite by adding whiskers to a fiber reinforced ceramic composite. The addition of whiskers to a continuous fiber ceramic composite has been shown to produce a hybrid composite that: (1) is more stiffer, (2) resists microcracking until higher loading levels, (3) has improved transverse strength and (4) shows improved damage tolerance when compared with fiber reinforced composites. Quantitatively, the modulus was found to be, on average, 212 ± 24 GPa for the hybrid system compared to 170 ± 20 GPa for the FCMC system. The ultimate strength was basically preserved, but the stress at which microcracking was first observed was increased for the hybrid system to 121.4 ± 19.0, an increase almost threefold over the FCMC system. The transverse microcracking stress was 31.0 ± 7.0 MPa for the HCMC compared with 16.4 ± 1.0 MPa for the FCMC. The ultimate strengths were

62.4 ± 7.0 MPa and 24.2 ± 6.0 MPa, respectively. The hybrid system was also seen to withstand more damage than the standard FCMC system. The study has indeed demonstrated the benefits from hybridization of ceramics and provide a basis for further study.

Personnel Supported

Dr. Lokeswarappa R. Dharani, Department of Mechanical and Aerospace Engineering and Engineering Mechanics served as the principal investigator on the project and Dr. Douglas R. Carroll, Basic Engineering Department served as a Co-PI. Several graduate and undergraduate students worked on the project supported either by AFOSR funds or the internal matching funds from the University of Missouri-Rolla. Thesese students are: (I) John E. Goethe, M.S.A.E. (1994), US Citizen, (ii) Stephen B. Haug, M.S.A.E.(1995) and Ph. D. A. E. Candidate, US Citizen, (iii) Mark A. Hall, M.S. M. E. Candidate, US Citizen (iv) Forrest W. Flocker, Ph. D. E. Mech. Candidate, US Citizen, (v) Paul R. Raj, M.S. E. Mech. (1995), Non-US Citizen, (vi) Fangsheng Ji, Ph. D. E. Mech. Candidate, Non-US Citizen, (vii) aaron E. Laws, B.S.A.E. (1994), US Citizen, (viii) Weiping Cai, B. S. Cer. E. (1995), US Permanent resident.

Interactions/Transitions

Results of this investigation have been presented at the following National conferences, Universities and Air Force Laboratory:

1. "Microcracking Stress and Transverse Properties of Hybrid Ceramic Matrix Composites," 18th Annual Conference on Composites and Advanced Ceramics Materials, Cocoa Beach, FL, January 9-14, 1994.
2. "Hybrid Ceramic Matrix Composites," Materials Directorate, Wright Laboratory, Wright-Patterson Air Force Base, March 21, 1994.
3. "Micromechanics Issues in Brittle Matrix Composites," Southern Illinois University, Carbondale, April 4, 1994.
4. "Hybrid Ceramic Matrix Composites," Aeronautical Development Agency, Bangalore, India, July 8, 1994.
5. "Hybrid Ceramic Matrix Composites: Processing and Characterization," Department of Mechanical and Aerospace Engineering and Engineering Mechanics, University of Missouri-Rolla, September 15, 1994.
6. "Hybrid Ceramic Matrix Composites: Processing, Characterization and Modeling," Ceramic Engineering Department, University of Missouri-Rolla, October 6, 1994.

One of the graduate students, John Goethe, worked with Wright Lab scientists in applying the Acoustic Emission technique to characterize damage evolution in hybrid ceramic matrix composites. The tape casting technique for making continuous fiber and hybrid composites was developed in consultation with the scientists at the Air Force Materials Directorate, WPAFB.

New Discoveries

Previous attempts to fabricate hybrid ceramic matrix composites have been limited to filament winding and hot pressing route. Hybrid composites fabricated via this route did not show any significant improvements in microcracking stress. This is primarily attributed to the inability of the slurry to infiltrate the fiber tows. The tape casting and hot pressing technique developed during this project holds much promise. Hybrid composites with very low porosity and highly uniform microstructure have been produced using tape casting and hot pressing route. This technique can potentially be used to fabricate ceramic systems that sinter at higher temperature than that of cordierite.

APPENDIX A

AN EXPERIMENTAL INVESTIGATION OF THE FAILURE MECHANISMS IN HYBRID CERAMIC MATRIX COMPOSITES

A Masters Degree Thesis in Aerospace Engineering

by

John Edward Goethe II

An Experimental Investigation of the Failure Mechanisms in Hybrid Ceramic Composites

By

John Edward Goethe II, 1970-

A THESIS

Presented to the Faculty of the Graduate School of the

UNIVERSITY OF MISSOURI-ROLLA

In Partial Fulfillment of the Requirements for the Degree

MASTER OF SCIENCE IN AEROSPACE ENGINEERING

1994

Approved by

Lokeswarappa R. Dharani, Advisor

Daniel S. Stutts

Douglas R. Carroll

ABSTRACT

A material system has been developed that employs the benefits of both fiber and whisker reinforcement in the strengthening and toughening of ceramics. It is the objective of this study to demonstrate the benefits of this hybrid system by means of flexure tests. It is shown that the hybrid material system will withstand a higher stress before microcracking occurs in the matrix; has improved transverse properties; and shows better damage tolerance when compared to ceramics reinforced solely with whiskers or fibers. Testing was performed in three point flexure using acoustic emissions analysis and microscopy techniques to map the progression of damage in the material systems.

Material properties and acoustic emission data are presented for three material systems: a whisker reinforced cordierite composite, a fiber reinforced cordierite composite and a fiber/whisker hybrid reinforced cordierite composite. This information was important in deducing the damage progression of the hybrid reinforced composite. Damage tolerance is shown by a detailed set of pictures identifying the different modes of failure. Occurance of damage was identified using a combination of acoustic emission analysis and microscopy methods. The hybrid composite system is shown to be 25% more stiff, have more than twice the transverse strength, have a higher stress before microcracking occurs and have better damage tolerance than the fiber reinforced ceramic composite system.

ACKNOWLEDGEMENTS

The motivation for the material system investigated for this project is the idea of my adviser, Dr. L. R. Dharani. I wish to thank Dr. Dharani for his advice and support and I am very pleased with my graduate school experience at the University of Missouri–Rolla under his guidance. I also wish to express thanks to Dr. D. R. Carroll and Dr. D. L. Cronin for their words of assistance as I pursued my next venture. Thanks also go to Steve Haug, Aaron Laws and Paul Raj for their work on the team. It takes the best efforts from everyone involved to make for a good research team, and your efforts did not go unnoticed.

I wish to extend my deepest appreciation to Dr. Ran Y. Kim, University of Dayton Research Institute, Wright–Patterson AFB, OH for letting us come and learn the methods that are currently being used in ceramic composites testing. To Dr. James G. Goree, Department of Mechanical Engineering, Clemson University, thank you for your generosity in letting us borrow the acoustic emissions analyzer used for the study. Without the help from these two men, the work for this project may not have been completed on time.

To all of my family and my best friend, Chad, thanks for your help and support. I hope that I will be able to give back to everyone what has been given to me. It is not without the support of these people that I could have done my best work.

TABLE OF CONTENTS

List of Figures

LIST OF FIGURES (CONT'D)

LIST OF TABLES

I. Introduction

The historical engineering desire to develop faster, stronger, lighter aircraft and automobiles and efficient engines has created the need to study advanced materials. The development of hypersonic aircraft, for instance, has resulted in the need for advanced materials that can withstand very high temperatures without a drastic loss in strength. Most lightweight metals cannot bear such high temperatures without experiencing a major change in microstructure. Ceramic based materials have become the materials of interest for such applications since they are more stable under higher temperatures than most metals can withstand. Even with the high temperature stability, ceramics tend to fail in a brittle fashion at relatively low stresses. Therefore, it is important to be able to engineer ceramic materials in order to improve their strength, toughness and damage tolerance.

It has been shown that reinforcing monolithic ceramics with long, continuous fibers greatly increases the strength and toughness of the material. Where the monolithic ceramic fails in a brittle manner, the continuous fiber reinforced ceramic typically displays a non-linear regime beyond the proportional limit in which the ceramic is capable of withstanding higher stresses before failure. Fiber reinforced ceramics have been shown to continue to carry load even after the matrix begins to crack. The properties normal to the fiber direction in the continuous fiber reinforced ceramic, however, become worse than the properties of the monolithic ceramic.

It has also been shown that reinforcing a ceramic material with small whiskers will increase the strength and stiffness of the material somewhat. This improvement in properties is mostly caused by the whiskers providing a

means of delaying onset of cracking in the ceramic and then deflecting or blunting the crack tip after cracking has begun. Previous research has shown that the whiskers are even able to bridge cracks in the material.

Under a project sposered by the U. S. Air Force Office of Scientific Research project at the University of Missouri–Rolla, studies are being conducted investigating the fabrication of ceramic composites reinforced by a combination of continuous fibers and whiskers, thus creating a "Hybrid Ceramic Matrix Composite (HCMC)". Once fabricated, these materials are being subjected to an exhaustive battery of tests in order to characterize their behavior under a variety of conditions. The objective of this work is to document the progression of damage in the HCMC during static flexure and define an experimental method for ceramic composites using acoustic emissions techniques and micrographic analysis. It is expected that the two types of reinforcement will combine to provide a stronger, stiffer material; increase the stress level at which the matrix begins to crack; increase the proportional limit and improve the transverse properties all without sacrificing the damage tolerance exhibited by the fiber reinforced ceramics.

In this thesis, the experimental method will be thoroughly explained, including a detailed explanation of the theory of acoustic emissions analysis. Following the experimental method, the material properties of the materials fabricated for this study will be presented with a detailed characterization of the progression of damage in the materials under stress. A collection of micrographs will also be presented as a means of illustrating the damage accumulation in the materials.

II. Review of Literature

There has been a significant amount of work performed showing the benefits of reinforcement in ceramic composites. Karandikar and Chou [1] investigated the damage evolution in continuous fiber reinforced composites with uniaxially oriented fibers and cross-ply lamina. Tredway, et al. [2] have presented results of high temperature tests for continuous carbon fiber reinforced mullite. Holmes [3], using silicon carbide reinforced calcium alumino silicate, has shown how continuous fiber reinforced ceramics exhibit "strain recovery" during high temperature creep testing. These researchers and many others have all well established the benefits derived from reinforcing ceramics with continuous fibers. Lin, et al. [4] showed that reinforcing a monolithic ceramic with whiskers improved flexural strength, fracture toughness and elastic modulus of ceramics. Other work has been performed showing the same results on different single reinforcement material systems [5]. Lewinsohn [6] has presented results of tests performed on hybrid fiber/whisker reinforced glass which showed improved transverse toughness. In each of the aforementioned work, information on testing methods has also been noted. Previous work in this field has been performed using both three point and four point bend tests almost equally.[2,4–6]

In addition, a means of detecting the occurrence of matrix microcracking has been investigated. Acoustic emission analysis techniques have become a popular means of attempting to observe cracking in a number of different materials. Background information on acoustic emissions was found in papers by Awerbuch [7]; Wevers et al. [8] and Higo and Inawa [9]. Kander [10] used

acoustic emissions monitoring techniques to study damage accumulation in unidirectional glass reinforced epoxy in static three point flexure. Faudree, et al. [11] studied the damage and fracture processes in short fiber bulk molding compound. In general, the previous research using acoustic emissions analyses has been performed on reasonably large specimens and several sensors are used in order to locate the source of the acoustic emission. The beneficial information obtained from Kander and Faudree, et al. was the logic used in tuning the acoustic equipment for successful testing results. Resource information on the Physical Acoustic Corporation PAC 3400 Acoustic Emissions Analyzer was obtained from a master's thesis by Wolla [12]. Wolla used the acoustic emissions analyzer to locate and map the growth of longitudinal cracks in a continuous fiber composite system. Using a combination of acoustic sensors, the source of each acoustic event can be determined based on the difference in time necessary for each sensor to record each event. Practical ideas for experimental application of acoustic emissions techniques were obtained as a result of a visit with Dr. Ran Y. Kim, University of Dayton Research Institute, at Materials Directorate, Wright Laboratory, Wright–Patterson AFB, OH.

III. EXPERIMENTAL

A. MATERIALS

All of the specimens used for this study were fabricated at the Materials Research Center on the campus of the University of Missouri–Rolla. The matrix material was processed from Cordierite frit purchased from Ferro Specialty Glasses, Cleveland, OH. The silicon carbide fibers used were provided in the form of sigma fiber mats by Atlantic IMT, Wilmington, MA. For the hybrid composite system, silicon carbide whiskers purchased from Third Millennium, Knoxville, TN, were substituted for 20% of the matrix powder. The properties of all of the constituents used for the different material systems investigated as a part of this study are summarized in Table I. WCMC, FCMC and HCMC represent whisker, fiber and hybrid reinforced ceramic matrix composites respectively.

Table I: Properties of Individual Constituents for WCMC, FCMC and HCMC systems.

Constituent	Density (g/cc)	E (GPa)	Strength (MPa)
Cordierite matrix	2.60	118	98
Sigma Fibers	3.40	410	3.45
SiC whiskers	3.20	580	8.30

(Properties compiled from Ceramic Source 1992–1993)

Table II: Measured and Theoretical Densities for the Investigated Material Systems.

Material System	Theoretical Density (g/cc)	Measured Density (g/cc)	Porosity (%)
WCMC	2.72	2.62	3.68
FCMC	2.79	2.67	4.3
HCMC	2.84	2.68	5.63

The specimens were produced using the tape casting method. In general, layers of ceramic tape were cast on plate glass with a doctor blade. Ceramic tape used for the hybrid composites were cast with whiskers mixed into the slurry. Continuous fibers, when used, were imbedded into the green tape. To make the final wafer from which the specimens were cut, layers of tape were then stacked into a mold and hot pressed in argon at 6.89 MPa and 950°C. Following hot pressing, the specimens were heat treated according to the schedule provided by Ferro. Cross sections of continuous fiber and hybrid specimens are shown in Figures 1 and 2. More detailed information on the processing of these composites is provided by Haug [13]. The resulting densities of the composites fabricated by the tape casting method for this study are summarized in Table II.

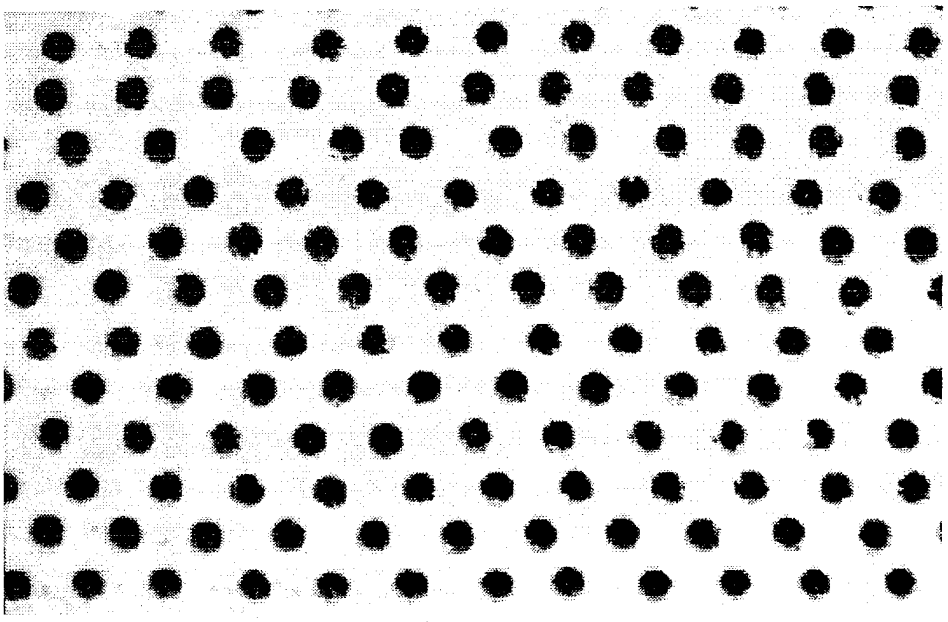

Figure 1: Optical image of the cross section of a typical fiber reinforced ceramic composite. Fiber diamater is 104 μm.

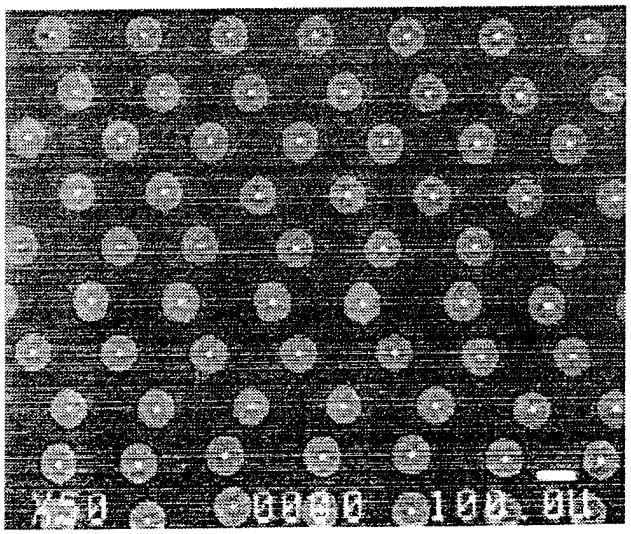

Figure 2: SEM micrograph of the cross section of a typical hybrid reinforced ceramic composite.

B. Experimental Setup

A block diagram of the experimental configuration is shown in Figure 3. All testing was performed on an MTS 810 load frame equipped with a 458.20 Microconsole, 458.11 Controllers for Load and Stroke and a 458.91 Microprofiler used to program the test. Data was taken from the controller electronics using a PC–XT set up to use the PC Lab software supplied by MTS Corporation. An x-y plotter was also used to obtain a qualitative load-displacement plot while the test was in progress. The load frame has a capacity of 97.9 kN. The 89.0 kN capacity load cell was used with a 8.9 kN cartridge for the load controller. The testing was performed in stroke control. The 13 mm sensitivity cartridge was used with the stroke controller. The testing was run at 0.076 mm/sec. This load rate was settled upon after some

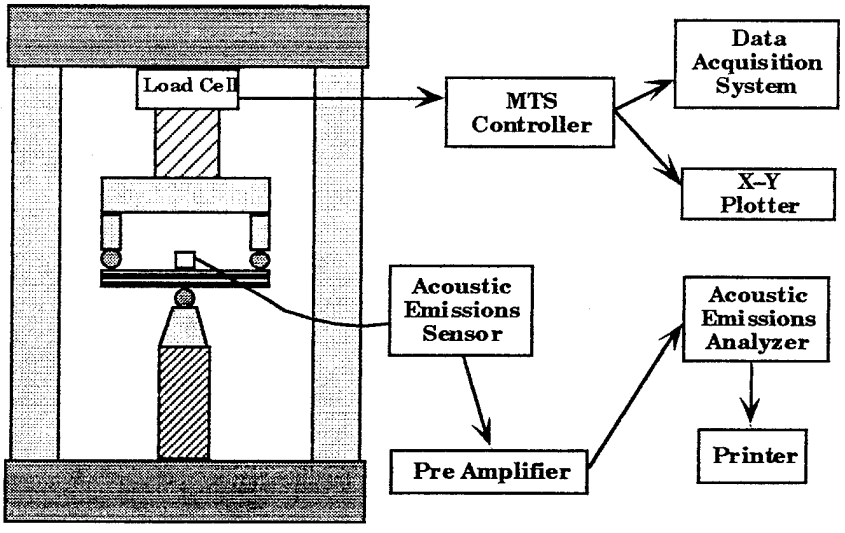

Figure 3: Experimental setup showing load frame configuration and acoustic emissions arrangement.

trial testing to set the time at which the material broke at between two and three minutes. There does not appear to be a standard for the load rate. This rate happens to be inside the window in which other research seems to fall.

The acoustic emissions analysis was performed using a PAC model 3400 produced by Physical Acoustics Corporation, Princeton, NJ. One channel was used with a piezoelectric transducer having a natural frequency of 150 kHz. A 40 dB PAC model 1220–A preamplifier containing a 100–300 kHz bandpass filter was used. Attached to the acoustic emissions analyzer was a serial printer used to obtain a list of the data acquired during the test. The software used with the system was the Real Time Data Acquisition System (RT/DAS) version 1.14. To be consistent with previous literature, the machine was configured to display the amplitude for each event. Extra information also obtained by the machine included rise time, duration, energy and number of counts read for each event. This data was displayed on the system screen histograms. The graphical representation of the data was not obtainable using the available printer however. Instead, the data was printed out in list form.

A Nikon Epiphot metallurgical microscope was also needed for the experiment. This microscope was used in conjunction with the acoustic emissions equipment to verify the nature of events occurring during testing. The microscope was equipped with a 35mm camera and exposure control electronics; polarizing lenses; reticles appropriate for measurement of crack densities and a variety of combinations of light filters. The light source was a 12 V 50 W Xenon bulb. Most useful to the microscopic investigation for this

project were the 20X and 40X objective lenses that accompanied the microscope. The microscope also had available 5X and 100X objectives.

Post testing microscopy was performed using a JEOL–330A scanning electron microscope. Specimens for which the extent of fiber pullout was desired were sputter coated with 150 nm of gold-palladium alloy. Specimens for which crack branching and microcracking were of interest were left uncoated. Investigations were performed using accelerating voltages of 10 and 15 kV.

C. Background on Acoustic Emissions

The detection of acoustic emissions for the purpose of monitoring damage has been the focus of many researchers for the past twenty years. The theory is that, as a material is put under load, strain energy is built up in the material. When the material fails, this strain energy is released as a wave through the material. Depending on the frequency of the released wave, the wave may or may not be audible. In either case, the wave can be detected using a transducer. It is believed that the properties of the wave that is detected can be directly related to the type of material being loaded, or, in the case of composites, the type of failure occurring. As a result, the PAC model 3400 is designed to measure the amplitude, energy, rise time, duration and number of counts for each particular event that occurs during the testing of materials.

An event is defined as the total "hit" on the transducer during a particular preset time step. This definition, then, allows for the differentiation

between an event and a count. An count is simply one hit on the transducer; and several counts may occur during one time step. To illustrate this idea, consider a crowd applauding a performance. At a certain instance in a performance, the audience might respond in applause. The instance of applause would be like an event. The number of times each person in the audience claps his hands would be a count. Other parameters such as duration, amplitude, energy and rise time can also be referenced to the applause example. For the materials used in this study, the frequencies of the events are above the audible range. The amplitudes range from 40 to 95 dB. The rise times are measured in microseconds and the durations are typically fractions of milliseconds. The number of counts can be multiples of thousands.

D. Experimental Procedure: Specimen Preparation

Bend specimens were cut from 40 mm long wafers using a low speed diamond saw so that the approximate cross section for continuous fiber and hybrid specimens were rectangles 3 mm by 4 mm. This cross section is consistent with previous work performed on ceramics in flexure. [4–6] The intent for a cross section of this size is to have a depth to span ratio of 1:10 or so and avoid "short beam" effects. Specimens used for determination of transverse properties and behavior were cut to have a cross section 3 mm by 6 mm. At the time of this work, there does not exist ASTM standards for testing of ceramic composites. The increase in the width for the transverse specimens was derived from ASTM D-3552 [14] for transverse properties in

metal matrix composites. Figure 4 shows the geometry of both the axial and transverse test specimens.

Since one component of the investigation of the failure mechanisms involved with the composites which are the focus of this study is the use of an optical microscope, the smoothest possible finish on the surface on the tension

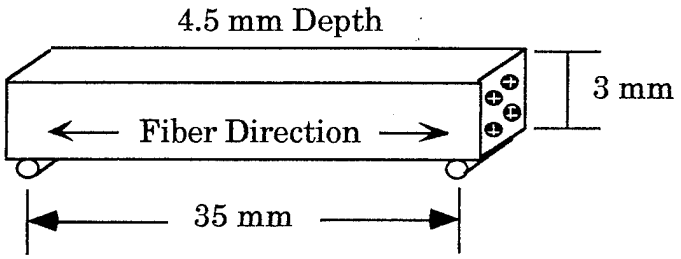

Axial Property Specimens
Samples: Neat Matrix, WCMC, CFCMC, HCMC

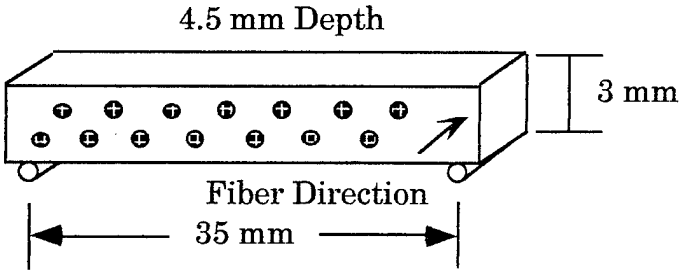

Transverse Property Specimens
Samples: CFCMC, HCMC

Figure 4: Axial and transverse specimens.

side of the beams must be attained. In addition, since much of the initial cracking occurs near the free edges of the specimens, the specimens should have corners as sharp as possible. Rounded corners are impossible to focus using an optical microscope. The method found to give the best results was to

polish the wafer from which the specimens were cut before cutting. Polishing was begun by "wet sanding" using 600 grit silicon carbide paper. As the quality of the surface improved, the particle size of the sanding medium was decreased. A 15 micron metal bonded diamond wheel was used without a sanding fluid. The final step in the polishing sequence was a buffing pad with a 0.6 micron alumina suspension. It was also decided that care should be taken not to polish as far as the first layer of fibers. If the first layer of fibers was exposed, it was observed that some of these fibers were usually damaged.

E. Experimental Procedure: Testing

There is extensive information that is needed to be recorded to provide for an exhaustive damage history for composite materials. In addition to documenting the onset of microcracking, the stresses at which fibers slip or fracture and occurrences of delamination, the progression of damage such as the microcrack density or crack spacing also needs to be noted at different stress levels throughout the range of loading. The need for this information requires an active use of the optical microscope throughout the experiment. Each time the specimen is viewed with the optical microscope, it is important to clean the specimen with ethanol or acetone since any oils or grease on the specimen can cover up cracks and make focusing the image of the specimen difficult.

Each time a new specimen is investigated, before it is mounted on the load frame, it was thoroughly examined with the optical microscope to note the extent of damage, if any, left after specimen preparation. The specimen was

then carefully mounted on the testing machine. The acoustic transducer was carefully fixed to the center of the specimen and held in place by placing a piece of Scotch™ tape over the sensor and attached to the bend fixture. Testing was performed using the prescribed load rates and paused every five to ten pounds of loading in order to check the damage accumulation. In the event of significant changes in the acoustic activity, the test would also be paused and the specimen investigated for damage. This process allowed for a reasonably successful correlation between the acoustic activity and damage phenomena; successful bracketing of the microcracking stress; and acceptable characterization of the damage history. Each time the test was paused, it was necessary to completely unload the specimen and remove the specimen from the load frame in order to inspect it microscopically.

Several consequences had to be considered as an aside to the experimental procedure. The first set of considerations involved the acoustic emission configuration. It was found that it was necessary to let the hydraulic pump on the testing machine run for a considerable time in order to let the fluid in the pump warm up to it's operating temperature (150 °F) and let the fluid equilibrate at this temperature. When this was not done, there was considerable acoustic activity detected by the sensor not related to the test. The coupling between the sensor and the specimen was also a concern. Previous work presented on acoustic emissions analysis [7–12] indicates that high viscosity vacuum grease creates a good acoustic interface between the sensor and the specimen. For this investigation, since the project relied heavily on optical microscopy, the vacuum grease was not used. It was found that a

medium used between the sensor and specimen was sometimes difficult to clean off and thus caused images from the microscope to be difficult to focus. The possibility that the coupling medium could fill in cracks was also a concern as, due to the nature of the metallographic microscope, it was then possible that cracks could be covered by the medium. The added consequence of this decision is the possibility that the sensor sliding on the specimen would create acoustic activity that would be avoided with the vacuum grease acting as a lubricant. Ultimately, it was determined that any increase in acoustic activity caused by the decision not to use vacuum grease was not appreciable. The final concern relating to the acoustic emissions system was the size of the sensor used. The available sensors were 10 mm in diameter. This size is significantly larger than the specimen width and the overlapping area of the sensor could conceivably register acoustic emissions from the surroundings of the specimen. The oversized sensor also would have been difficult to be "acoustically coupled" with the specimen if vacuum grease had been used. Based on the consistency of the testing, even though a smaller sensor is still preferred, the results obtained using larger sized sensor were acceptable.

Rubber pads were considered for use in this experiment between the specimen and the contact points of the bend fixture. The purpose of these pads would be to: (1) isolate the specimen from vibrations in the system caused primarily from the hydraulics, and (2) reduce damage on the surface of the specimen resulting from the contact between the specimen and the steel fixture. The rubber used in early runs of the experiment was obtained from sectioned pieces of a vacuum cleaner drive belt. While the two purposes for

which the rubber was sought were attained, the rubber still was not as stiff as necessary and the resulting load–displacement curves reflected the non-linearity caused by the presence of the rubber. An increase in the acoustic activity was definitely noticed after the elimination of the rubber, but the acoustic emissions threshold and amplification parameters were able to be adjusted to not register this activity. Changing the threshold and amplification in order to achieve this result causes the acoustic emissions equipment to be less sensitive. The concern then arises as to if acoustic activity is not detected that should be. To account for the loss in acoustic emissions that occurs with the analyzer adjusted to be less sensitive, the frequency of removing the specimen from the load frame to look for cracks with the microscope was increased.

One last concern in the performance of this experiment as outlined is the possibility that, as the material is loaded and unloaded for the purpose of using the optical microscope intermittently during the test, the material would experience a reduction in strength and a change in behavior due to fatigue. In the event that fatigue caused a degradation in the overall stress–strain behavior of the materials, the first and last specimens from each set of tests were run without stopping the test to get a complete stress–strain curve. This curve was then used as a guide to what would be expected for materials for which the damage history was determined. It is expected that, as cracks develop, the modulus of the material will decrease each time the specimen is unloaded and then reloaded. This effect, itself, is often used to determine the progression of damage in ceramics.

IV. Results from Testing

A. Material Properties

Three material properties that naturally follow from extensive testing of ceramic composite materials are (1) Young's modulus, (2) First microcracking stress and (3) ultimate strength. The average values for these properties for all of the material systems involved in the investigation are summarized in Table III. Five specimens were tested for the whisker reinforced composite system (WCMC). Ten specimens were tested for the continuous fiber reinforced composite system (FCMC) while six specimens were tested for the hybrid fiber/whisker reinforced system (HCMC). Three tests were performed to determine transverse properties for the continuous fiber reinforced composite system and four tests were performed for the hybrid system to determine transverse properties. The number of tests was based principally on the consistency of the data obtained from the tests. A wider scatter in the data necessitated more testing.

Table III: Summary of Material Properties

Material System	Volume Fractions		E_{11} (GPa)	First Microcracking Stress (MPa)	Ultimate Strength (MPa)
	Fiber %	Whisker %			
Neat matrix	0	0	118 ± 10	98 ± 10	98 ± 10
WCMC	0	20	159 ± 12	45.4 ± 2.5	210.5 ± 27
FCMC	30	0	170 ±20	47.3 ± 8	380 ± 45
HCMC	30	15	212 ± 24	121.4 ± 19	380 ± 30

Table IV: Summary of Transverse Properties

Material System	Volume Fractions		E22 (GPa)	First Microcracking Stress (MPa)	Ultimate Strength (MPa)
	Fiber %	Whisker %			
Neat matrix	0	0	118 ± 10	98 ± 10	98 ± 10
WCMC	0	20	159 ± 12	45.4 ± 2.5	210.5 ± 27
FCMC	15.8	0	69.5 ± 14	16.4 ± 1	24.2 ± 6
HCMC	15.8	15	131 ± 14	31.0 ± 7	62.4 ± 7

From Table IV, the result of adding randomly oriented whiskers to the matrix to create the hybrid reinforcement increased the axial stiffness by 25%, but almost doubled the transverse stiffness. More significantly, the transverse strength of the HCMC system was more than doubled compared to the FCMC system simply by adding the whiskers to the matrix.

B. Damage Characterization

A monolithic ceramic material, under load, will tend to break, without warning, at its failure load. Reinforced ceramic materials will tend to crack at loads significantly lower than their failure loads, but maintain their capacity to hold increased loads until final failure. This phenomenon is known as microcracking. The most important goal of this investigation was to determine precisely when the materials of choice in this study began to exhibit microcracking, document the progression of damage following the onset of microcracking and then deduce the contribution of each element of the

material in resisting damage. The focus of this study was a newly developed fiber/whisker reinforced (hybrid) ceramic composite. In order to deduce the contribution to damage tolerance of the individual constituents of this composite, it is necessary also to investigate the results of reinforcing the base ceramic with whiskers alone and with fibers alone.

By reinforcing the base ceramic with 20% by volume 1 μm diameter silicon carbide whiskers, a material is obtained that is more than twice as strong and is 32% more stiff than the base ceramic. It has been observed during this study, that, at small loads, striations develop in the whisker

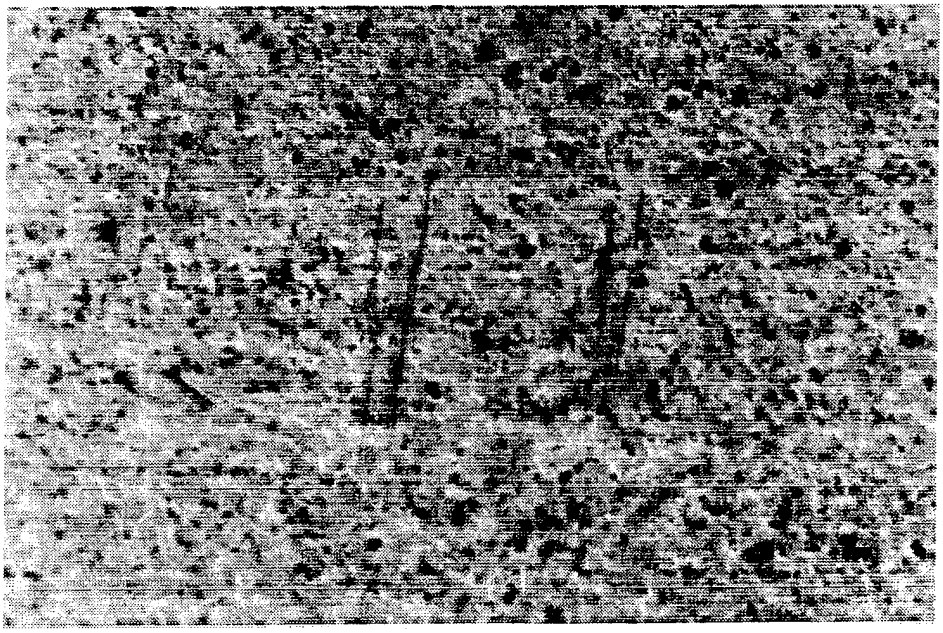

Figure 5: Striations in a typical whisker reinforced composite at the onset of microcracking magnified 400X, tension side of the specimen.

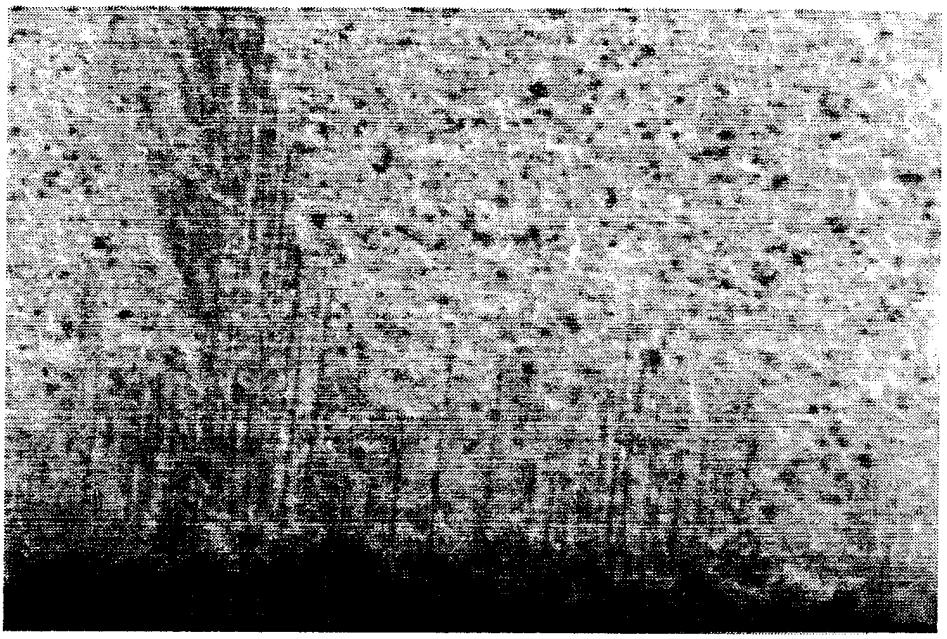

Figure 6: Striations in a typical whisker reinforced composite at 114 MPa magnified 400X, tension side of the specimen.

reinforced ceramic (WCMC). These striations have been found to produce acoustic emissions with amplitudes 40 ± 5 dB. Striations, such as those shown in Figure 5 at a magnification of 400X, typically appear in the WCMC at a stress level of 45.4 ± 2.5 MPa. The density of striations increases noticeably at a stress level of 114 ± 2 MPa. A typical representation of this increase in striation density is shown in Figure 6 at a magnification of 400X. From the stress–strain plot shown in Figure 7, there does not appear to be a proportional limit present in the stress–strain curve generated from static testing. Rather, the material fails in a brittle fashion typical of ceramics without a non - linear response. This behavior indicates that the whiskers, randomly

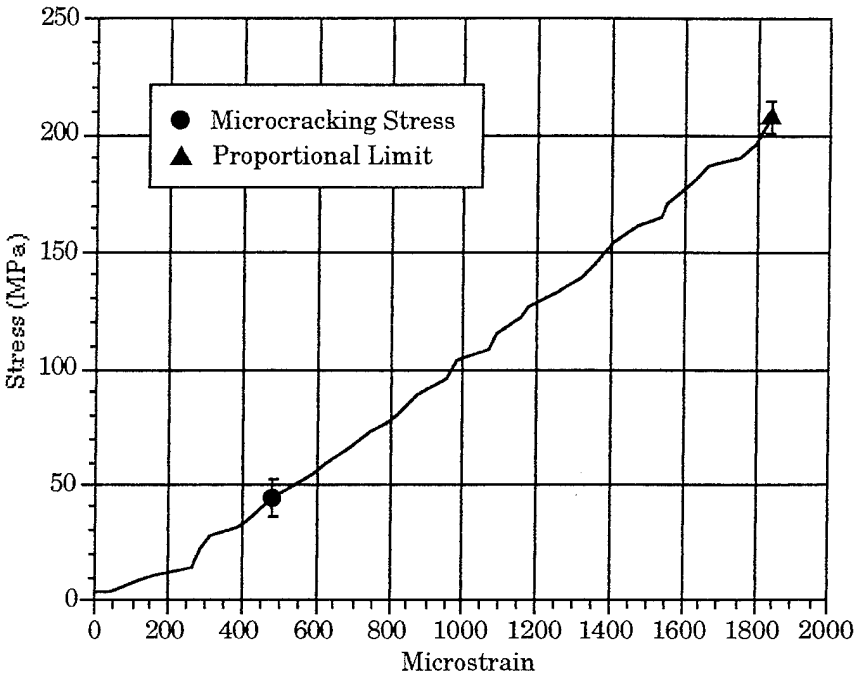

Figure 7: Stress–strain curve for a typical whisker reinforced ceramic composite.

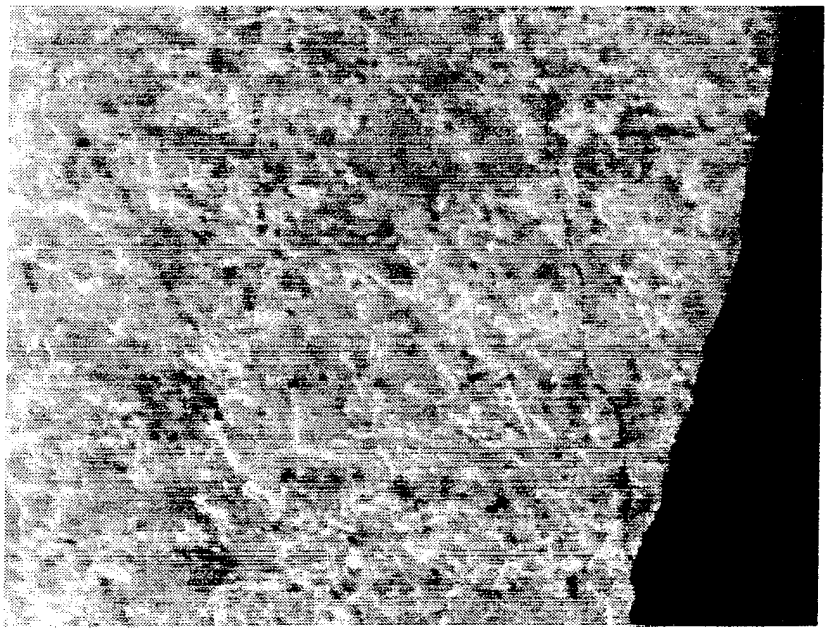

Figure 8: Post failure fracture of a typical whisker reinforced composite, tension side.

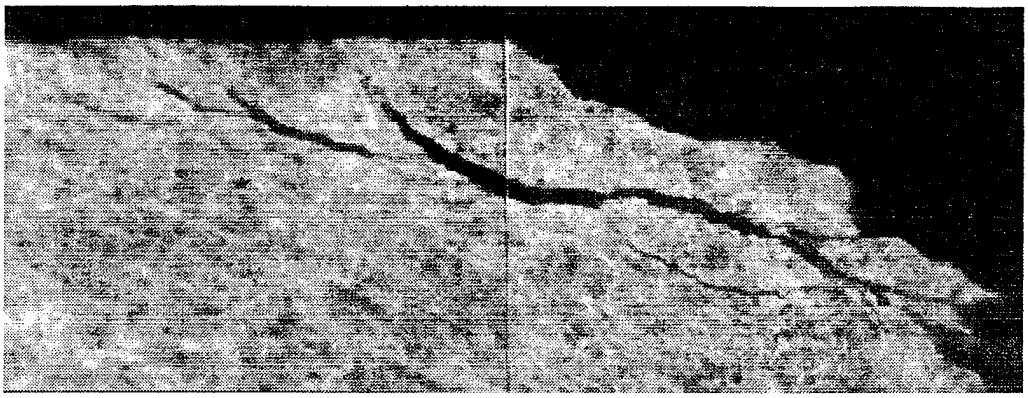

Figure 9: Crack branching in a whisker reinforced composite, tension side.

oriented, serve to strengthen the base ceramic and not to provide for damage tolerance. The strengthening mechanism likely arises from the whiskers increasing the modulus of the composite, and thus, reducing the stress in the matrix.

From post–failure observation of the WCMC, it also appears that the whiskers promote crack branching in the composite. Figures 8 and 9 show instances of crack branching in the WCMC after failure at a magnification of 400X. Intuitively, when a crack approaches a whisker, the most likely path in which the crack will grow will be either parallel to or almost exactly perpendicular to the whisker. Also, intuition would hold that a crack would be deflected away from regions of high concentrations of whiskers, since energy considerations for crack growth support the notion that cracks will grow along the paths of least resistance. It is difficult to state conclusively based on Figures 8 and 9 the explanations for the paths that the cracks in the two figures have taken since all that can be seen in the figures is the outer face of

the specimen and whiskers beneath the outer layer are likely oriented differently. However, the fact that branching exists to the degree shown indicates the positive contribution of whiskers added to the ceramic. There are several regions in both figures that illustrate the intuitions of crack growth in whisker composites.

Reinforcing a monolithic ceramic with continuous fibers presents a much more radical means of strengthening compared to the use of whiskers. From a production standpoint, it seems to be much more difficult, based on the results of testing during the present investigation, to attain consistent lamination strength, bond strength and distribution from product to product. The distribution of the fibers also tends to be important in that two fibers should never touch. The volume fraction for the fiber reinforced composites

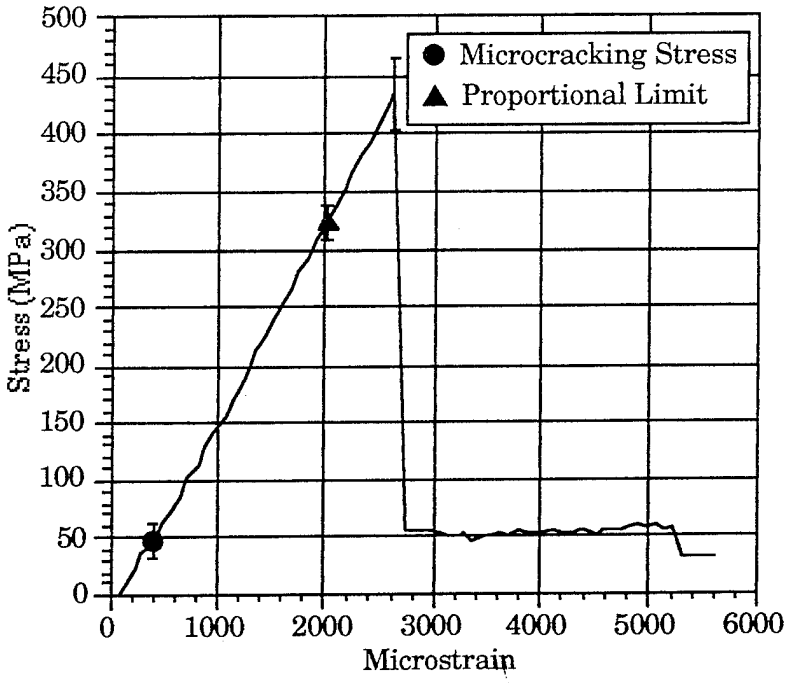

Figure 10: Typical stress–strain curve for fiber reinforced ceramic composites.

(FCMC) tested was a minimum of 28.14% and a maximum of 32.62%. The fibers used for reinforcement in these composites were 104 mm in diameter. The resulting composite is, on average, 30% more stiff than the monolithic ceramic and as much as 4.5 times stronger, in the direction parallel to the fibers. The main disadvantage to reinforcing the monolithic ceramic with continuous fibers is the strength transverse to the fiber direction, which is only 25.3 MPa, about 25% of that of the monolithic ceramic. A typical stress–strain curve for a fiber reinforced ceramic is shown in Figure 10.

The damage progression displayed by the continuous fiber composite is important in the investigation of the damage evident in the hybrid materials. There are several different mechanisms involved in the load carrying capabilities of fiber composites. Besides the matrix and fibers individually cracking, the fibers are known to debond and slip in the matrix, thus dissipating energy through friction. These three mechanisms can each be differentiated using the acoustic emissions analyzer. Summarized in Table V, it was found that acoustic emissions were consistently detected with amplitudes of 44 ± 2 dB for matrix cracking, amplitudes of 51 ± 2 dB indicating fiber slippage and

Table V: Acoustic Emission Amplitudes for the Different Failure Events in Ceramic Composites.

Event	Acoustic Amplitude (dB)
Matrix Cracking	44 ± 2
Fiber Slipping	51 ± 2
Fiber Breakage	62 ± 2

62 ± 2 dB for fiber breakage. In all cases, the initial energy release resulting in the formation of a major crack and catastrophic failure in the composite (that is, the point at which the specimen first experiences a sharp decrease in load carried) caused an acoustic event with amplitude greater than 90 dB.

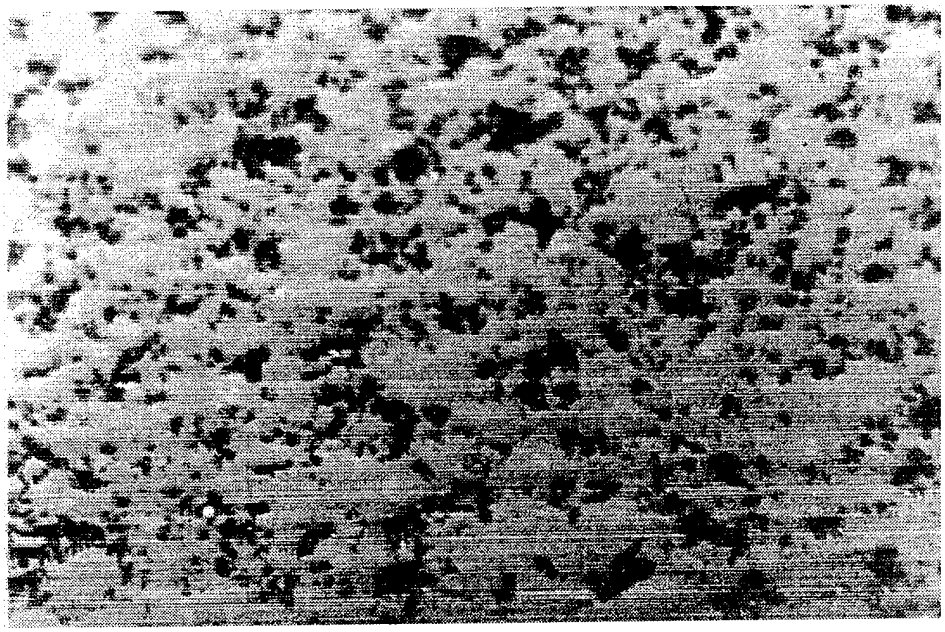

Figure 11: Polished surface of a fiber reinforced ceramic composite before loading, tension side of the specimen.

Similar to the whisker composites, at early stages in the loading, the fiber composites will tend to crack. The microcracking is best illustrated by Figures 11 and 12. Figure 11 shows a typical "polished" region of FCMC before the specimen is loaded at a magnification of 400X. After polishing, there are typically pits in the surface of the specimen, but any scratches in the specimen caused by cutting are polished out of the surface. Figure 12 shows

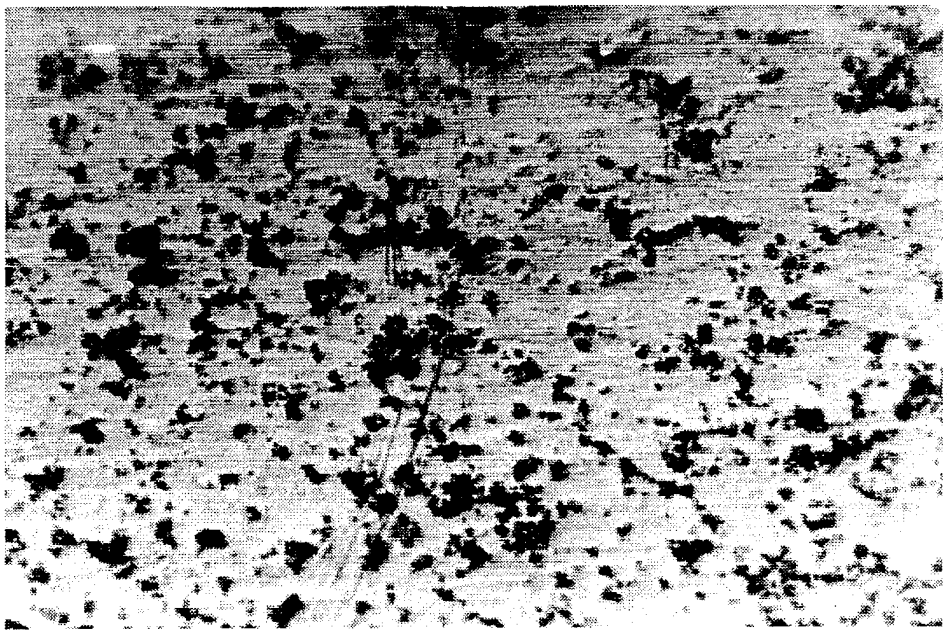

Figure 12: Microcracking in a typical fiber reinforced ceramic composite at a stress level of 46 MPa magnified 400X, tension side of the specimen.

Figure 13: Cracking in a fiber reinforced ceramic composite at a stress level of 200 MPa, tension side of the specimen.

an example of cracking that occurs at the instance of first acoustic emission detection at 400X. For the FCMC system in this study, the microcracking occurs around 45 MPa . As the loading is increased, the spacing between cracks becomes smaller until the material finally fails. Figure 13 shows a region in the FCMC at stresses closer to the failure load. The progression of crack density for the FCMC system of this study is best documented with the graph in Figure 14. After the microcracking stress, the cracks appear closer together in an exponential fashion until failure.

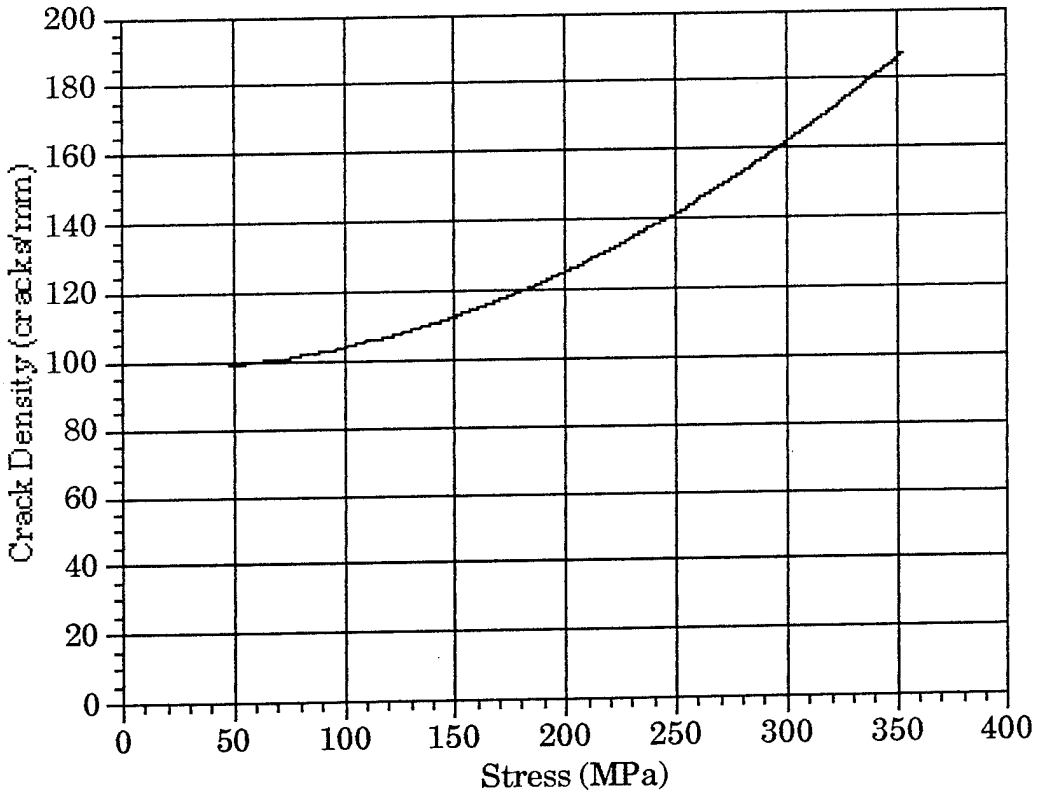

Figure 14: Crack density propagation for fiber reinforced ceramic composites.

Most of the time, the FCMC system used in this study did not display a distinct proportional limit. However, based on acoustic emissions studies, the debonding and slipping of fibers tended to occur about 300 MPa, between 15 and 20% beneath the maximum load held by the specimen. Following "catastrophic failure", the material still typically held a load 10 to 15% of the maximum load held. After an initial sharp drop in the loading, this load was approached asymptotically as the major crack progressed through the material.

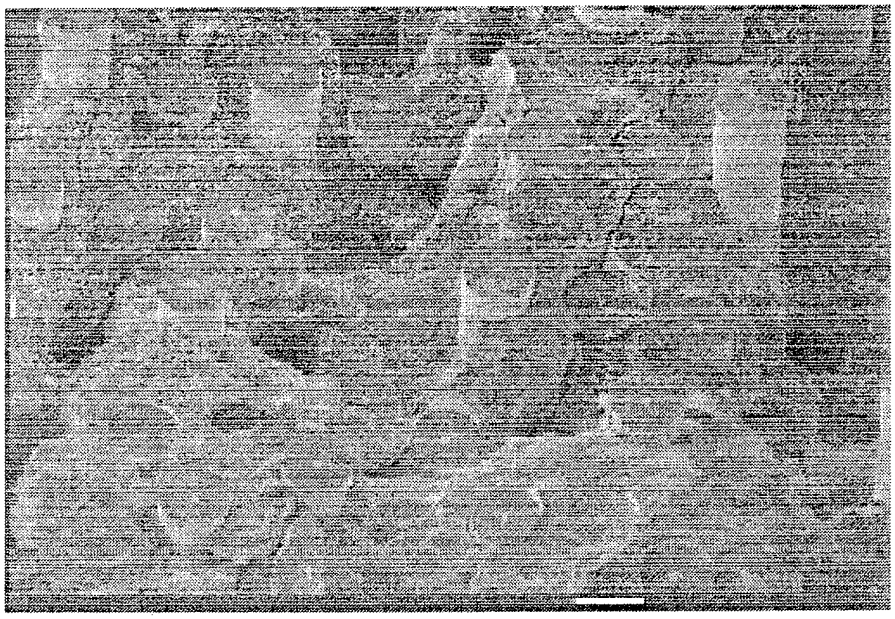

Figure 15: Fractograph of a fiber reinforced ceramic composite.

Figures 15 and 16 show an examination of the cross section of the material using scanning electron microscopy. Of main interest is the progression of cracks that appear to run parallel to the fibers as "interlaminar"

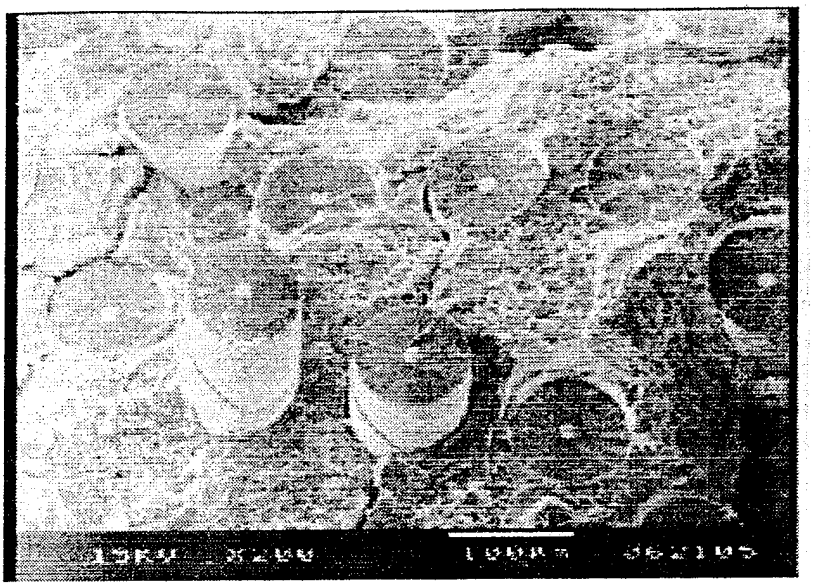

Figure 16: Fractograph showing interlaminar cracking in bottom center of fiber reinforced composite shown in Figure 15.
(micron bar is 100 μm.)

Figure 17: Fractograph showing fiber pull–out in a continuous fiber reinforced ceramic composite system.

cracks. Figure 15 shows a particular area in a typical FCMC sample at 100X. Note the crack that runs from bottom left to upper right. In general, the fibers along this crack are not pulled out. The fibers exhibiting the largest degree of pull–out are not involved with any laminar type cracks. Figure 16 shows the bottom center of the picture in Figure 15 at a magnification of 200X. The micrograph in Figure 16 serves to highlight these interlaminar cracks. In both of these figures, the tension side of the beam is to the right of the micrograph. In Figure 15, there exist two cracks which are parallel to each other. Figure 17 shows another region on the same sample showing fibers that have "pulled out". Fiber pull–out is desired since the frictional interface between fibers that have debonded and slid serves to dissipate energy and allows the material to tolerate damage.

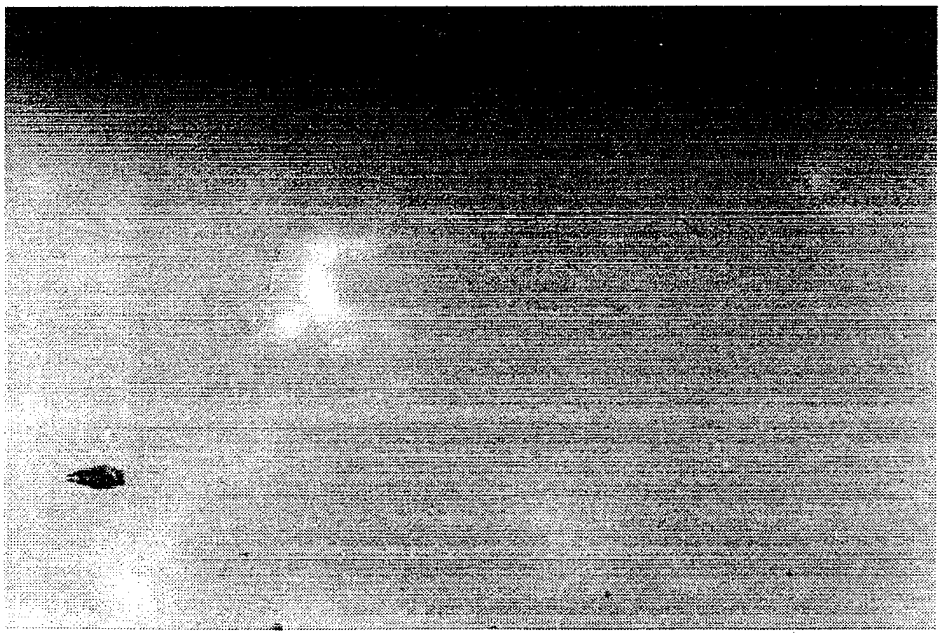

Figure 18: Highly polished face of a transverse fiber reinforced ceramic specimen, tension side.

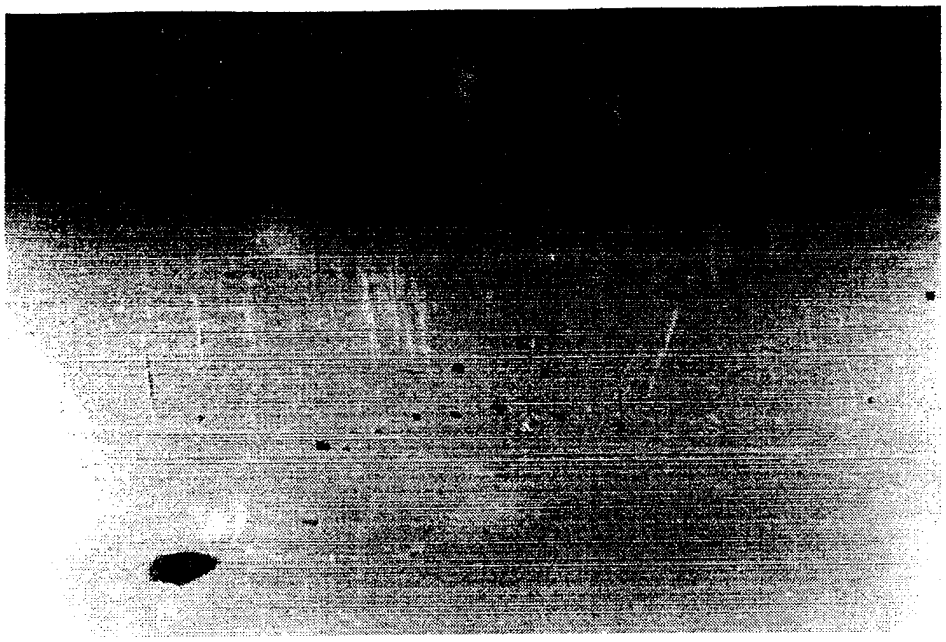

Figure 19: Microcracking evident in tension side of transverse fiber reinforced ceramic composite specimen at a stress level of 25 MPa magnified 400X.

Examination of the transverse behavior of the FCMC system shows the distinct contrast in behavior compared to the response in the axial direction. The transverse specimens first exhibited microcracking at a stress level of 16.5 ± 0.1 MPa. The strength of the material in the transverse direction was only 25 MPa. In general, the microcracking behavior of the material was similar to that of the whisker composite. Figure 18 shows a sample of a well polished transverse FCMC specimen. Figure 19 shows the striations evident at the inspection declaring the microcracking stress level. Because the ultimate strength of the transverse composites is small, microcracking does not tend to be very widespread. In the process of loading, striations as shown will develop and shortly later the specimen will break. Striations tend to

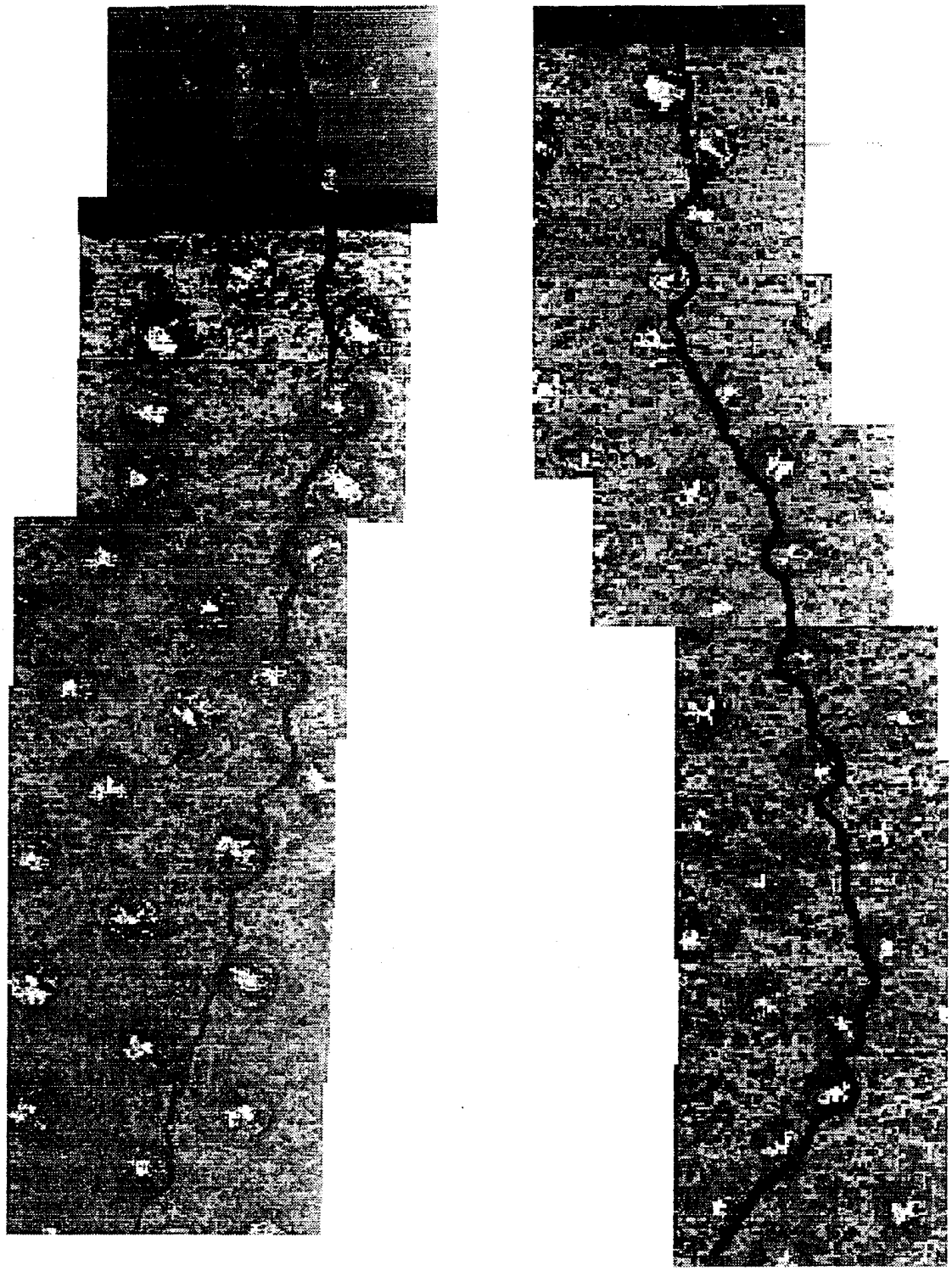

(a) (b)

Figure 20: Map of the major crack in different transverse fiber reinforced ceramic composite specimens.

develop predominantly near the free edges of the composite. Cracking does not tend to occur away from the free edges until the specimen fails catastrophically. Typically, at catastrophic failure, two or three cracks will develop with approximately a 50 micron spacing on either side of the major crack.

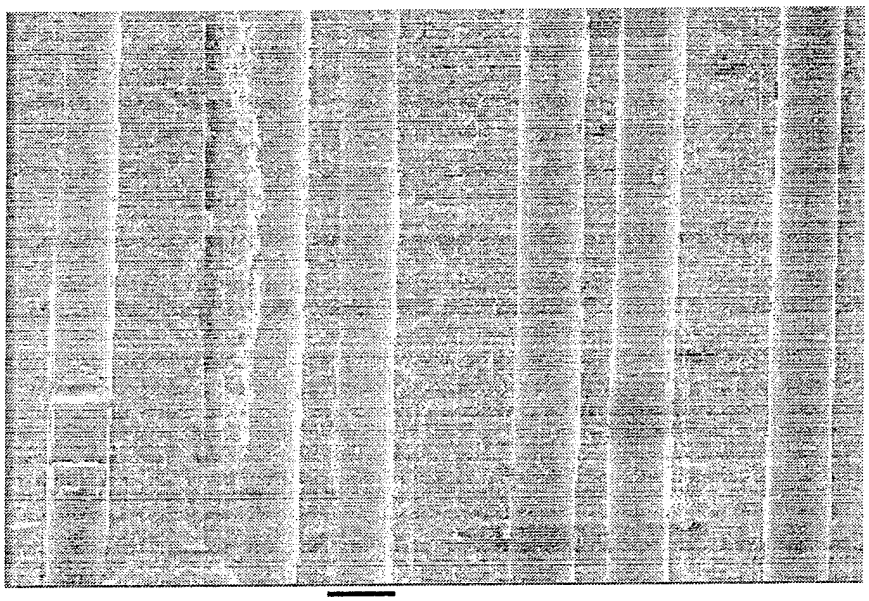

Figure 21: Fractograph of a transverse fiber reinforced ceramic composite.

Further insight to the cracking of the FCMC specimens might be gained from the post–failure examination of the transverse specimens looking parallel to the fibers. Almost without fail, the crack grows in a manner connecting the fibers. This fact is intuitive if the fibers are not well bonded to the matrix. In

fact, the crack likely grows connecting debonded fibers. Figures 20 (a) and (b) show separate instances of such crack growth in the transverse FCMC specimens. Figure 21 is a SEM micrograph of a transverse FCMC specimen. The most notable observation to be made with this figure is the regular clean breaks around fibers.

Having set the foundations of the independent contributions of fibers and whiskers in the reinforcement of ceramics, the failure mechanisms evident when the two reinforcements are combined can now be explained. As has been established with the other material systems, as the hybrid reinforced composite (HCMC) is loaded, at some load lower than its proportional limit, the

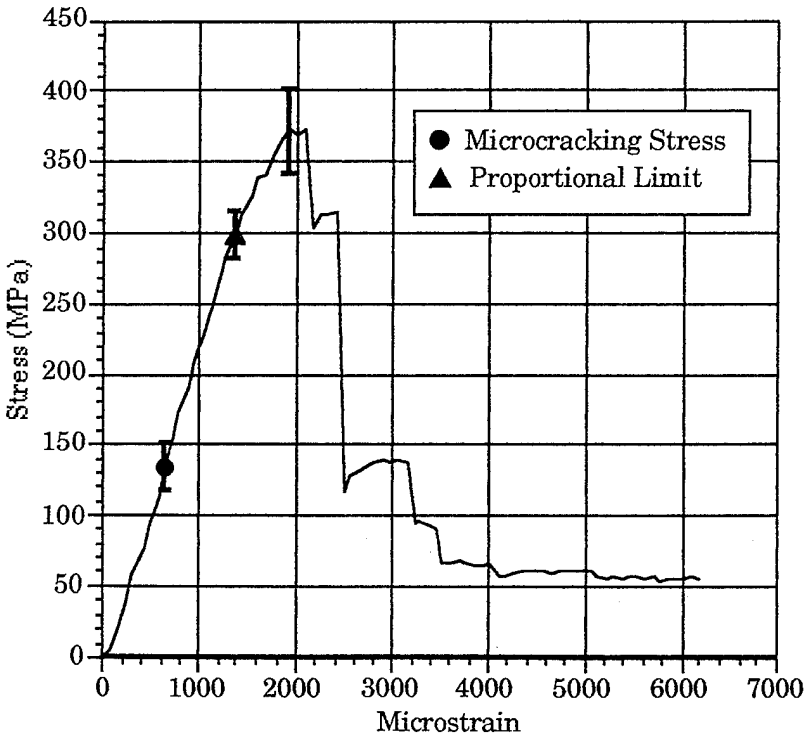

Figure 22: Stress–strain diagram for the hybrid reinforced ceramic composite system.

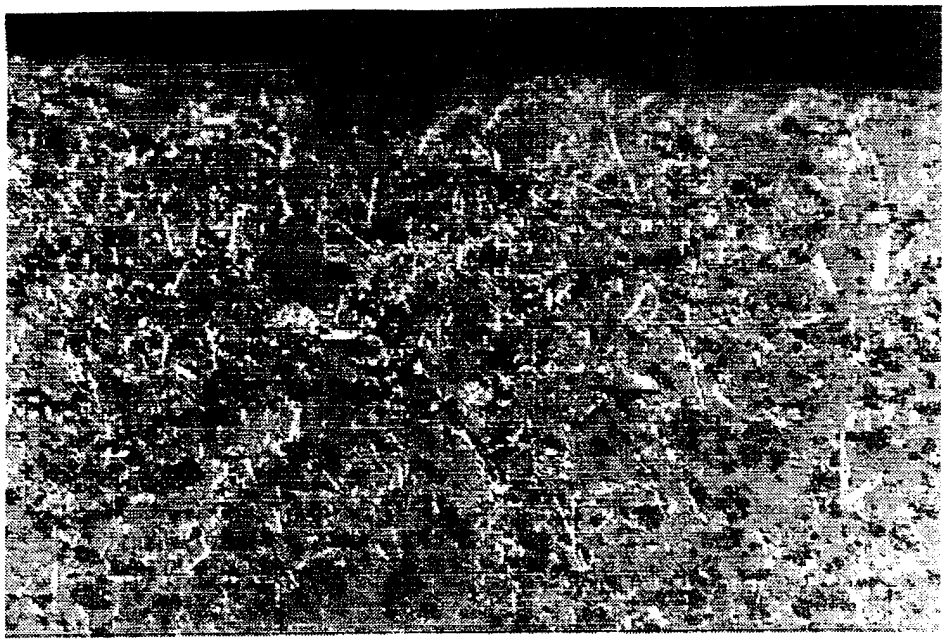

(a)

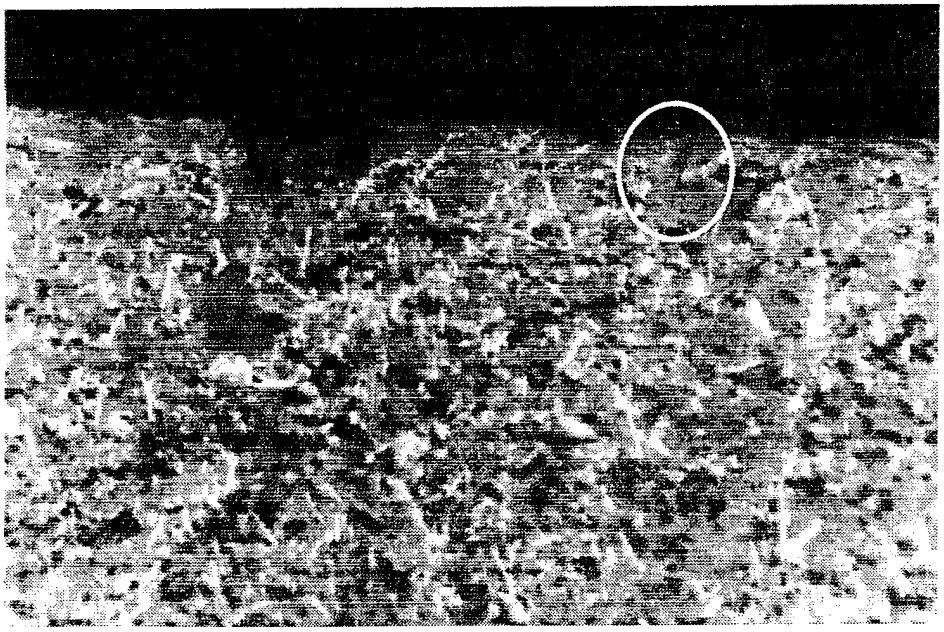

(b)

Figure 23: Polished surface of tension side of hybrid reinforced composite before and after first acoustic emission.

material will begin to crack or develop striations similar to those previously shown. Although magnitude of ultimate and microcracking stresses from specimen to specimen was not very consistent, the microcracking stress for the HCMC system was consistently 35.6% ± 2% of the ultimate strength of the material. This result corresponds to a stress of 129.3 ± 12 MPa. A typical stress–strain curve for the HCMC system is shown in Figure 22. On average, the ultimate strength of the HCMC specimens was approximately the same as the ultimate strength of the FCMC system. Hence, adding the whiskers to the FCMC system provides much greater resistance to microcracking in the matrix. The acoustic emissions detected from the loading of the hybrid composite specimens corresponded well with the amplitudes noted from the

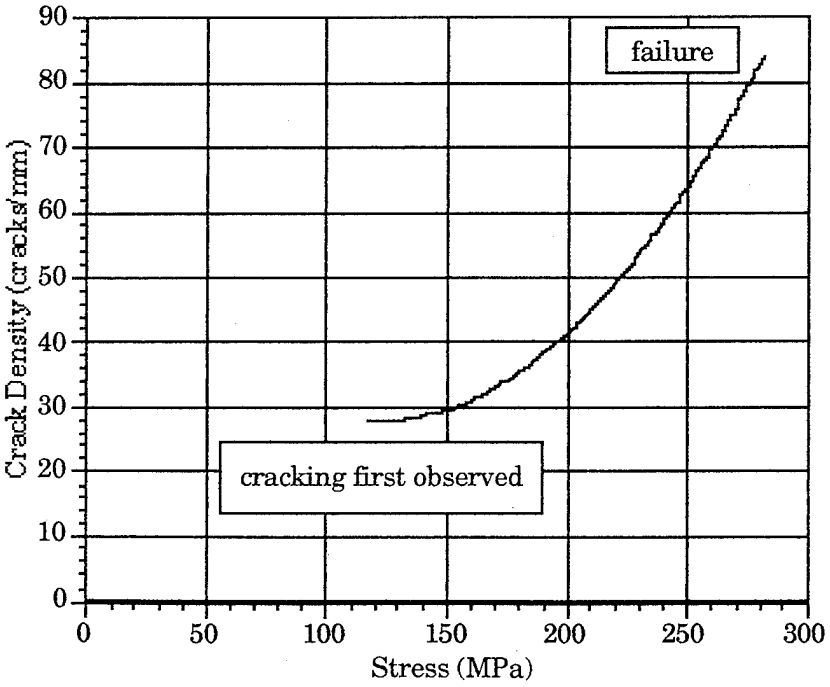

Figure 24: Crack density growth for hybrid reinforced ceramic composite system under load.

Figure 25: Path of major crack in a transverse hybrid reinforced ceramic composite specimen.

testing of the WCMC and FCMC systems. Figure 23 (a) shows a sample area on the tension side of a polished HCMC specimen before testing. Figure 23 (b) shows the same region in the same sample after the first acoustic events detected. Note the occurance of a crack on the top edge of the specimen to the right of the smaller edge defect. The density of the cracks increases in a manner shown by the graph in Figure 24. The trend is similar to the trend shown in Figure 14 for the FCMC system.

The toughening effect of the whiskers in the matrix can also be seen from examination of the transverse hybrid specimens. The ultimate strength of the HCMC system loaded in a direction transverse to the fibers was 62.5 ± 7.3 MPa. The stress at which microcracks were first discovered on the specimen was, on average, 31.0 ± 7.2 MPa, almost twice that of the FCMC loaded transversely. An examination of the path of the major crack developed at the point of "catastrophic failure" may also provide some useful insight. The composite picture shown in Figure 25 shows the path of a typical major crack progressing through the thickness of a transverse HCMC specimen. In sharp contrast to the cracks shown in Figures 21 (a) and (b), there is not nearly the extent of debonding around fibers, and hence, the crack tends to travel more of a straight line path through the specimen. There exist fibers around which the crack had to progress, but, unlike the FCMC system, the crack does not necessarily connect the fibers. There is evidence of a crack eminating from a possibly debonded fiber near the center of the photograph, but this seems to be the only such instance. The behavior illustrated from the examination of this transverse specimen crack supports the notion that, by adding whiskers to the

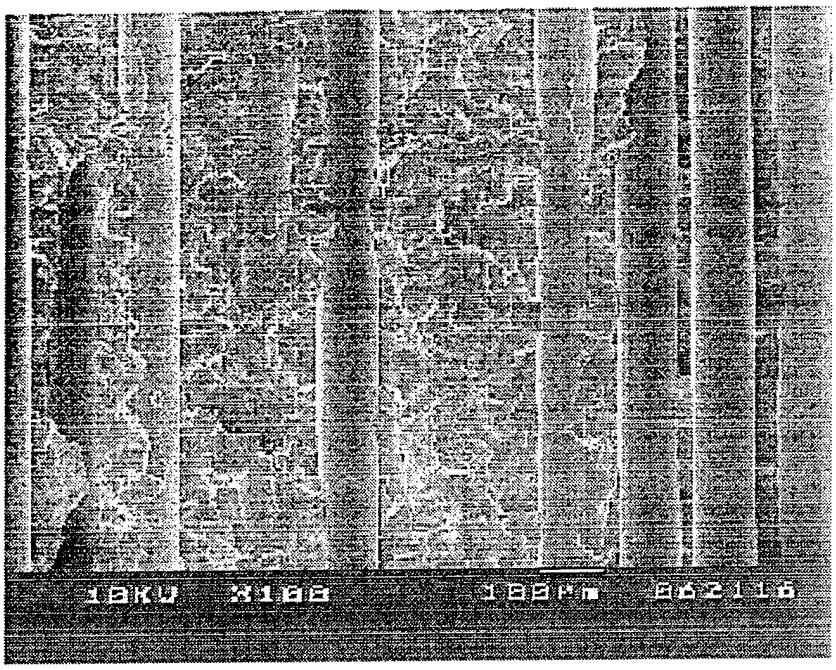

Figure 26: Fractograph of a transverse hybrid reinforced ceramic composite.

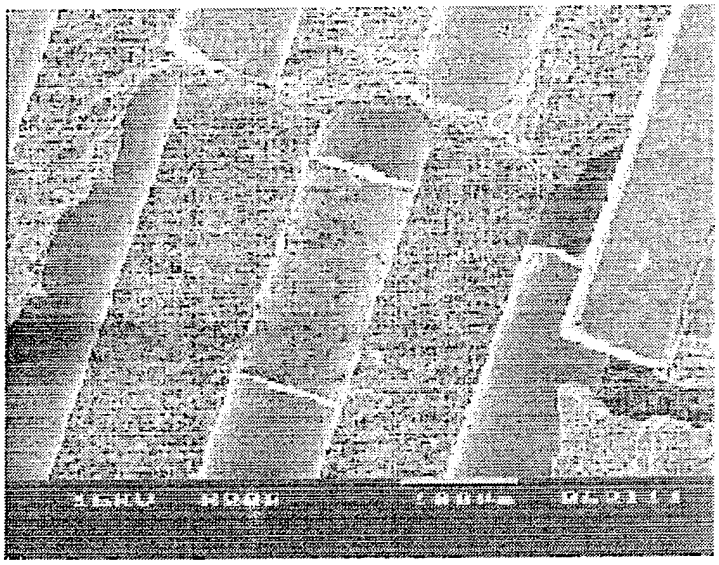

Figure 27: Fiber of a hybrid reinforced ceramic composite that is experienceing pull–out. (The micron bar is 100 μm.)

matrix of the FCMC, the fibers are more tightly gripped and a better interface between the fibers and matrix is the result. The micrograph shown in Figure 26 also shows effects of the whiskers in a transverse HCMC specimen after fracture. Note that the matrix now shows some topography and the fracture is not as smooth as the fracture shown in Figure 20. Such topography is indicative of crack deflection through the matrix which contributes to damage tolerance in the material.

Further investigation of the HCMC specimens tested with the fibers oriented in the direction of loading provides additional insight into the mechanisms that may occur during the cracking of the HCMC system. Figure 27 is a SEM micrograph showing a fiber that has broken and had

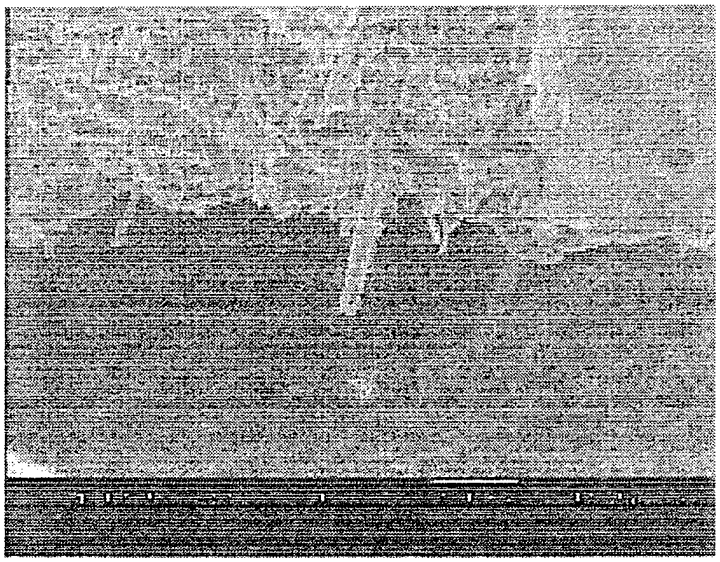

Figure 28: Whiskers protruding from a matrix region in a hybrid ceramic composite sample. (The micron bar measures 10 μm.)

undergone some pull–out before the loading was stopped. This effect is one of the most important toughening mechanisms in this HCMC system. Typically, the fiber pull-out effect is reflected in the stress–strain curve as a non-linear segment of the curve. The micrograph shown in Figure 28 shows, at relatively high magnification, the protrusion of whiskers out of a matrix region fairly close

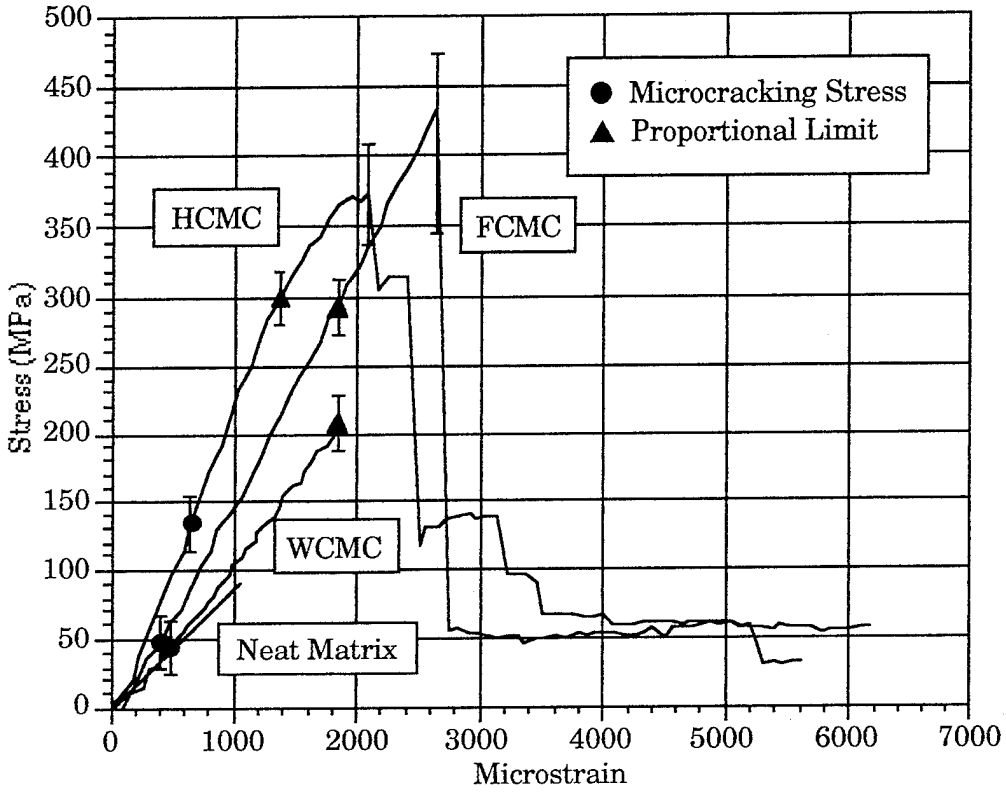

Figure 29: Stress–strain curves for all of the ceramic material systems involved in the study.

to the region on the sample shown in Figure 27. Notice that the whiskers are oriented at a variety of angles coming out of the matrix. So called whisker pull-out also contributes to non-linear behavior in the stress–strain curve similar to

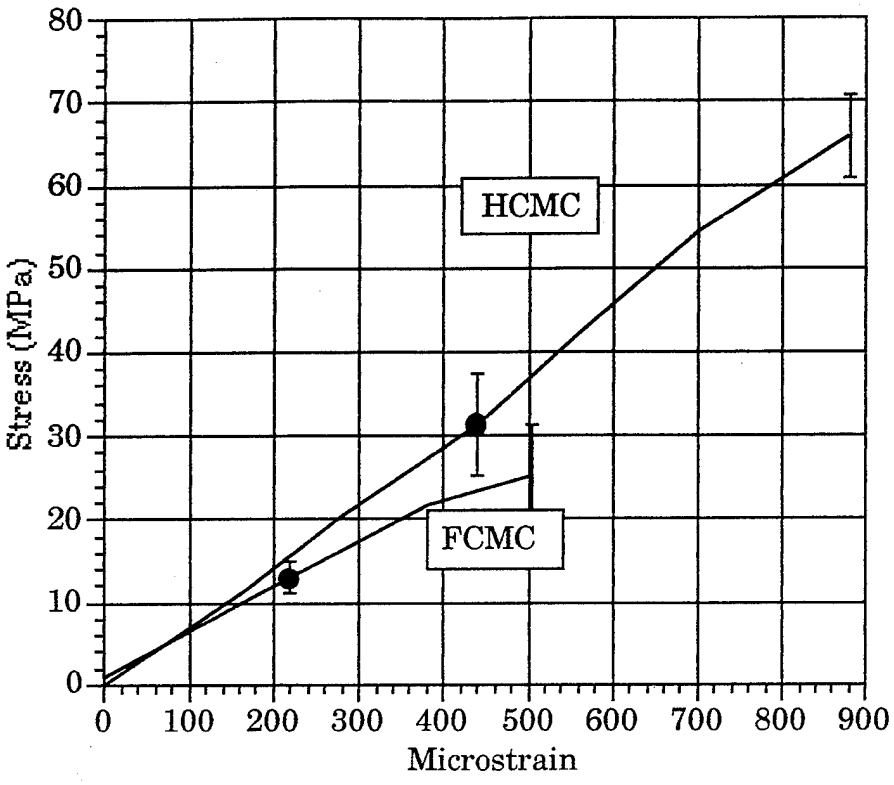

Figure 30: Stress–strain curves for transverse property specimens.

the effect from fiber pull-out. Having the whiskers oriented in several directions and still exhibiting pull-out also is beneficial in the toughening of the material system.

In order to further illustrate these results, Figure 29 is presented showing the stress–strain curves for all of the material systems investigated in the study superimposed upon each other. Note that, although the ultimate strength of the HCMC and FCMC systems tested are nearly equivalent, the inconsistency between specimens prevents conclusive remarks therein. The HCMC clearly exhibits damage tolerance not seen in the FCMC. The ledges evident in the HCMC curve after "catastrophic failure" are levels in the

straining of the composite where the major crack has run and then stopped and proceded parallel to the fiber direction. Each dropoff in the curve at higher strain levels represents one or more layers of fibers ultimately fracturing. In the process of testing the HCMC system, not once was the material able to be broken in two. Rather, at some point in the loading, the crack continued to run parallel to the fiber orientation indefinitely. Provided in Figure 30, for completeness, is the collection of stress–strain curves obtained for the transverse property specimens.

V. Conclusions and Future Work

The purpose of this study was to demonstrate the effects, and ultimately, the advatages of forming a hybrid ceramic composite by adding whiskers to a fiber reinforced ceramic composite. The addition of whiskers to a continuous fiber ceramic composite has been shown to produce a hybrid composite that: (1) is more stiff, (2) resists microcracking until higher loading levels, (3) has improved transverse strength and (4) shows improved damage tolerance when compared with strictly fiber reinforced composites. Quantitatively, the modulus was found to be, on average, 210 ± 30 GPa for the hybrid system compared to 153 ± 25 GPa for the FCMC system. The ultimate strength was basically preserved, but the stress at which microcracking was first observed was increased for the hybrid system to 129.3 ± 12, an increase almost threefold over the FCMC system. The hybrid system was also seen to withstand a good amount more damage than the standard FCMC system. The data and pictures presented clearly show benefits from hybridization of ceramics and provide a basis for further study.

The work presented is solely the result of static flexure tests. There is much more work that needs to be completed in order to show all the benefits of this means of hybridization for ceramic composites. Tests need to be performed in tension, creep, high and low cycle fatigue and under extreme conditions. Concurrent work involves interfacial strength investigation by means of fiber push-out tests and further development of the fabrication process. As all of this work is completed, this means of hybrid reinforcement should be the foundation for the next generation of ceramic composites.

BIBLIOGRAPHY

[1] Karandikar, P. and Chou, T. W., "Characterization and Modeling of Microcracking and Elastic Moduli Changes in Nicalon/CAS Composites," Composite Science and Technology, Vol. 46, pp 253–263, (1993).

[2] Tredway, W. K., Prewo, K. M., Isosa, T., Iwata, M., "Performance of a Carbon Fiber Reinforced Mullite Matrix Composite," Proc. of the 6th Japan–U.S. Conference on Composite Materials, pp 351–359, (1992).

[3] Holmes, J. W., "Fatigue of FIber Reinforced Ceramics," in Ceramics and Ceramic Matrix Composites, S. R. Levine (ed.), ASME, New York pp 193–238, (1992).

[4] Lin, G. Y., Lei, T. C., Zhou, Y., Wang, S. W., "Mechanical Properties of Al_2O_3 and Al_2O_3 + ZrO_2 Ceramics Reinforced by SiC Whiskers," Journal of Materials Science, Vol. 28, pp 2745–2749, (1993).

[5] Goto, Y. and Tsuge, A., "Mechanical Properties of Unidirectionally Oriented SiC–Whisker–Reinforced Si_3N_4 Fabricated by Extrusion and Hot–Pressing," J. Am. Cer. Soc., Vol. 76 No. 6, pp. 1420–1424, (1993).

[6] Lewinsohn, L. A., "Hybrid Whisker–Fiber Reinforced Glass–Matrix Composites with Improved Transverse Toughness," J. of Material Science Letters, Vol. 12, pp. 1478–1480, (1993).

[7] Awerbuch, J., "On the Identification of Failure Mechanisms in Composite Laminates through Acoustic Emission," in Acoustic Emission, J. Eisenblätter (ed.), DGM Informationsgesellschaft Verlag, Oberursel, Germany, pp 47–58, (1988).

[8] Wevers, M. I., Verpoest, P., De Meester and Aernoudt, E., "Identification of Fatigue Failure Modes in arbon Fiber Reinforced Composites with the Energy Discriminating Acoustic Emission Method," in Acoustic Emission: Current Practice and Future Directions, ASTM STP 1077, W. Saschse, J. Roget and K. Yamaguchi (eds.), American Society for Testing and Materials, Philadelphia, (1991).

[9] Higo, Y. and Inawa, H., "The General Problems of AE Sensors," in Acoustic Emission: Current Practice and Future Directions, ASTM STP 1077, W. Sachse, J. Roget and K. Yamaguchi (eds.), American Society for Testing and Materials, Philadelphia, (1991).

[10] Kander, R. G., "A Study of Damage Accumulation in Unidirectional Glass Reinforced Composites via Acoustic Emission Monitoring," Polymer Composites, Vol. 12, No. 4, pp 237–245, (1991).

[11] Faudree, M., Baer, E., Hiltner, A. and Collister J., "Characterization of damage and Fracture Processes in Short Fiber BMC Coposites by Acoustic Emission," Journal of Composite Materials, Vol. 22, pp 1170–1195, (1988).

[12] Wolla, J., "Experimental Determination of the Fracture Behavior of Damaged Graphite/Epoxy Laminates and Comparison to the Shear–Lag Model," Master's Thesis, Clemson University Department of Engineering Mechanics, (1984).

[13] Haug, S. B., Dharani, L. R., and Carroll, D. R., "Fabrication of Hybrid Ceramic Composites," communicated to Advanced Composite Letters, (1994).

[14] ASTM D 3552–77, "Standard Test Method for Tensile Properties of Fiber–Reinforced Metal matrix Composites," (1982).

VITA

John Edward Goethe, II was born on September 2, 1970, in Freeport, Illinois. His family moved to Peoria, Illinois at age three and started his elementary schooling slightly more than one year later. In 1980, Mr. Goethe moved with his family to Harrisonville, Missouri where he completed the balance of his elementary and secondary education. He received a Bachelor of Science degree in Aerospace Engineering from the University of Missouri–Rolla in May of 1992, graduating magna cum laude.

Mr. Goethe remained at UMR to perform graduate studies. He was supported in his graduate work by a Chancellor's Fellowship. He was also awarded a departmental fellowship and worked as a Graduate Teaching Assistant, teaching Engineering Graphics for two years. He was supported during his two summers as a Graduate Research Assistant through a grant from the U. S. Air Force Office of Scientific Research.

APPENDIX B
FABRICATION OF CERAMIC MATRIX COMPOSITES BY TAPE CASTING AND LAMINATION

A Masters Degree Thesis in Mechanical Engineering

by

Stephen Berry Haug

FABRICATION OF CERAMIC MATRIX COMPOSITES

BY

TAPE CASTING AND LAMINATION

by

Stephen Berry Haug, 1962-

A THESIS

Presented to the Faculty of the Graduate School of the

UNIVERSITY OF MISSOURI-ROLLA

In Partial Fulfillment of the Requirements for the Degree

MASTER OF SCIENCE IN MECHANICAL ENGINEERING

1995

Approved by

Lokeswarappa R. Dharani, Advisor

Douglas R. Carroll

Terry F. Lehnhoff

ABSTRACT

The tape casting and lamination method was used to fabricate three different types of ceramic matrix composites. The material systems include continuous aligned silicon carbide fiber reinforced cordierite, partially aligned silicon carbide whisker reinforced cordierite and a hybrid ceramic matrix composite employing both aligned fibers and whiskers. Monolithic cordierite was also produced to verify the matrix properties. Sintering to near theoretical density for fiber volume fractions up to 35% was achieved by hot pressing. Measured fiber volume fractions were typically within 1-2% of the desired values. The purpose of this study was to develop a fabrication technique that provides predictable and consistent ceramic composite specimens.

Mechanical characterization was made by means of three point flexural testing with acoustic emission monitoring. Both continuous aligned fiber reinforcement and whisker reinforcement provide improvement in strength and stiffness over monolithic specimens. The hybrid system displayed significant improvement in transverse properties when compared to the continuous aligned fiber composite. The stress associated with the onset of microcracking in the matrix was substantially increased for the hybrid ceramic matrix composite.

ACKNOWLEDGMENT

For providing me with a project by which to develop my research and technical skills I wish to express my deepest appreciation and gratitude to my advisor Dr. L. R. Dharani. I would also like to thank the other members of my advisory committee, Dr. D. R. Carroll and Dr. T. F. Lehnhoff, for their guidance and words of wisdom throughout the course of this project.

Much deserved credit goes to Dr. M. R. Reidmeyer and Dr. J. W. Stevenson of the Ceramic Engineering Department for lending their technical expertise during the development of the tape casting process. I also recognize Dr. R. E. Dutton and Dr. Ran Y. Kim of the U. S. Air Force Materials Laboratory, Dayton, Ohio, for their advice in the processing and characterization of ceramic composite materials.

For their assistance in fabrication, specimen preparation and testing I extend my thanks to former graduate students Dr. Gopal Padmanabhan, John Goethe and Paul Raj; fellow graduate student Mark Hall and undergraduate assistants Aaron Laws, Scott Burrelsman and Scott Cargill.

This project was funded in part by the U. S. Air Force Office of Scientific Research (Grant #F49620-93-10223). The Manufacturing Research and Training Center (Missouri Department of Economic Development) provided a matching grant to supplement the AFOSR funding. The University of Missouri Research Board provided the seed grant used to conduct the feasibility study. I would like to thank Dr. Walter Jones, Program Manager, AFOSR, and Dr H. Dean Keith, MRTC, for their support of and cooperation with this project. I also thank Mr. Bill Hanusiak, Atlantic Research Corporation, for supplying the Sigma fiber mats at no cost.

CONTENTS

LIST OF FIGURES

LIST OF TABLES

I. INTRODUCTION

The present trends in the automotive and aviation industries are increasing the demands on the materials they use. The need to improve the efficiency of internal combustion and gas turbine engines is leading to higher temperatures and pressures, light weight components and reduced friction. The development of hypersonic aircraft will require materials that can withstand very high temperatures on their leading edges, external surfaces and engine components.

Ceramic based materials are leading candidates for high temperature components. Ceramics retain their strength and resistance to wear, creep and fatigue to higher temperatures than alloys[1]. Additionally, ceramics tend to be of low density, giving them high specific strengths. Presently the uses of ceramic materials are limited to components such as furnace insulation and elements, kiln furniture, cutting tools, insulators, oxygen sensors, filters, catalytic converter cores and electronic devices[1-3]. Light weight, porous, fused silica tiles and silicon carbide coated carbon-carbon composites are used for the exterior thermal management system of the Space Shuttle[4]. In the automotive industry ceramics are being considered for use in engine parts such as valves, rings, springs, bearings and seals[1,5]. Potential aerospace engine applications include advanced turbo ramjet (ATR) fuel regenerators, bipropellent rocket fuel injectors, gas turbine combustion chambers and stator vanes in addition to bearings, springs, seals and thermal insulating panels[1,6-10].

The brittle nature of monolithic ceramic materials prohibited their use in components for which catastrophic failure would prove disastrous. To be useful, ceramic components will need to withstand the accumulation of damage which occurs between inspection cycles and survive intact. They must be inspectable, so that damaged

components can be identified and replaced.

Reinforcing a brittle material with continuous fibers has been shown to increase it's strength and fracture toughness[11,12]. Continuous fiber ceramic matrix composites (FCMC) exhibit considerable toughness beyond the first matrix microcracking stress level. The microcracking stress corresponds to wide spread multiple cracking in the matrix. The improved toughness arises from the elastic energy of the fibers bridging the cracks, the energy required to break the fiber/matrix interface bond and the energy needed to overcome the friction encountered during fiber pull-out. Crack deflection during failure also enhances a material's fracture toughness[13]. Longer crack paths resulting from crack deflection increases the work of fracture.

Unidirectional FCMCs tend to have transverse (perpendicular to fibers) characteristics that are substantially inferior to the monolithic matrix properties. The improvement of transverse properties gained in using [0/90] composites is accompanied by diminished properties in the longitudinal (parallel to fibers) direction for a given amount of material, reducing it's longitudinal specific strength. The use of these bi-axial laminated composites also leads to other problems such as free edge delamination and interlaminar debonding.

Whisker reinforced ceramic matrix composites (WCMC) consist of either random, aligned or partially aligned discontinuous fine fibers dispersed in a ceramic matrix. WCMCs exhibit significant improvements in strength, elastic modulus and fracture toughness[14-16]. The use of randomly oriented whiskers yields a composite with isotropic properties. Anisotropic materials can be tailored by varying the degree of alignment of the whiskers. Using particulate and platelet reinforcement improves fracture toughness

but tends to reduce the elastic modulus and ultimate strength[17].

Using both aligned continuous fibers and dispersed fine whiskers to reinforce the ceramic matrix creates what is referred to as a hybrid ceramic matrix composite (HCMC). The goal of this work is to improve the transverse properties and microcracking stress of a unidirectional FCMC without compromising the original damage tolerance capability[18,19].

The project that formed the basis of this study required the fabrication of monolithic, WCMC, FCMC and HCMC specimens. The specific material systems used involved cordierite (magnesia alumino silicate or MAS) for the matrix with silicon carbide whiskers (SiC_w) and carbide fibers (Sigma SiC_f) as reinforcements.

The tape casting and fiber lamination method of fabricating ceramic matrix composites allows a more precise control over the material's microstructure than filament winding or powder processing. Volume fractions are consistent and are more accurately adjustable. Initial voids are small leading to low porosity in the final product. The result is a specimen that is uniform and closely represents theoretical models. This paper represents a detailed guide to the fabrication of CMCs using tape casting, lamination and hot pressing. An overview of the general procedures utilized to make CMCs can be seen in the block diagram depicted in Figure 1.

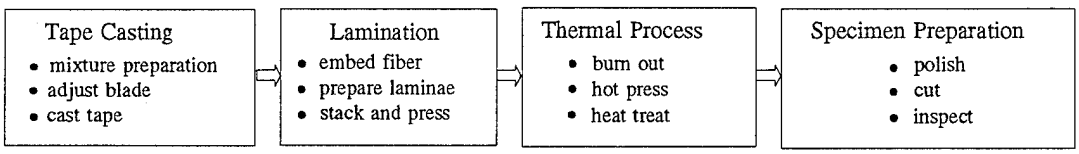

Figure 1. The sequence of processes used to fabricate CMC specimens.

II. REVIEW OF LITERATURE

The tape casting process has it's origin in the development of thick film technology and has been applied in the manufacture of electronic components, being used as dielectrics for multilayer capacitors, piezoelectric cells and substrates for multilayer integrated circuit packages[1,20]. Researchers from Aerojet and Cercom have successfully fabricated a monolithic silicon nitride ATR fuel regenerator containing intricate internal passages using tape casting, die punching, lamination and sintering[10]. Partially aligned platelet reinforced ceramic matrix composites have been produced by Claaßen and Claussen using tape casting and lamination[17].

The tape casting slurry must be tailored to a specific application. The constituents of the slurry must be chemically compatible with the ceramic powder. The relative quantity of dispersants, binder and plasticizers depend upon the surface area of the powder, which is a function of particle size, and the chemical adhesion between the binder and powder. Although the theoretical relationships exist, empirical methods are generally used to find the proper ratios of the slurry formulation. Compositions for mullite, alumina and mullite/alumina composites have been experimentally developed at UMR by Dr. M. R. Reidmeyer[21]. A similar process was used to make glass/fiber composites via tape casting and fiber lamination by Dr. R. E. Dutton at the U. S. Air Force Materials Laboratory[22].

Solvent based organic binder systems are preferred over aqueous based systems because they have been well developed and produce consistent results. The resulting green ceramic tapes have excellent properties such as strength, pliability and long shelf life. The particular system chosen uses the least hazardous solvents of available systems.

III. FABRICATION

A. TAPE CASTING

An ideal green ceramic tape will have the highest possible amount of glass/ceramic frit (powder) without being too brittle or sticking to the glass casting surface. If the powder loading is too low the resulting tape will be excessively visco-elastic and stretch immoderately when removed from the casting surface, leaving permanent wrinkles in the tape. If the powder loading is too high the tape will tend to stick to the casting glass and may have insufficient strength and pliability. The powder loading is typically between $65\%_{vol}$ and $70\%_{vol}$ in the green ceramic tape. Modifying the ratios of the binder and plasticizer also affects the strength, pliability and adhesion of the tape. Modifying the ratios of solvents changes the viscosity of the casting slurry and the drying rate. The recipe was experimentally developed for cordierite and the whisker/cordierite composite based on similar glass/ceramic compositions[21,22].

1. Mixture Preparation. The components of the formulation along with their functions are presented in Table I. The particle size for the cordierite frit as determined by sedigraph is $50\%_{wt} < 8$ to 10 micron[23]. The SiC_w were observed to be 0.5-2.5μm in diameter, from 15μm up to about 80μm in length and primarily single crystal. Since the whiskers are considered to be hazardous when friable[24] they were measured and introduced to the slurry under a ventilation hood. The particles and whiskers can be seen together in the secondary electron image (SEI) shown in Figure 2. Table IIa gives the composition of the cordier-ite tape and Table IIb gives the composition of the SiC_w reinforced cordierite tape.

Table I. Components of the tape casting formulations.

Commercial Name	Chemical Name	Function
cordierite (MAS)	magnesia-alumino-silicate	ceramic matrix
SiC_w	silicon carbide whiskers	matrix reinforcement
Butvar® (B-76)	polyvinyl butyral resin	binder
Santicizer® (S-160)	butyl benzyl phthalate	plasticizer
Carbowax® (PEG-400)	polyethylene glycol	release agent/plasticizer
Defloc™ (Z-3)	blown medhaden fish oil	dispersant
Toluene	toluene	solvent
Ethanol	ethyl alcohol	solvent

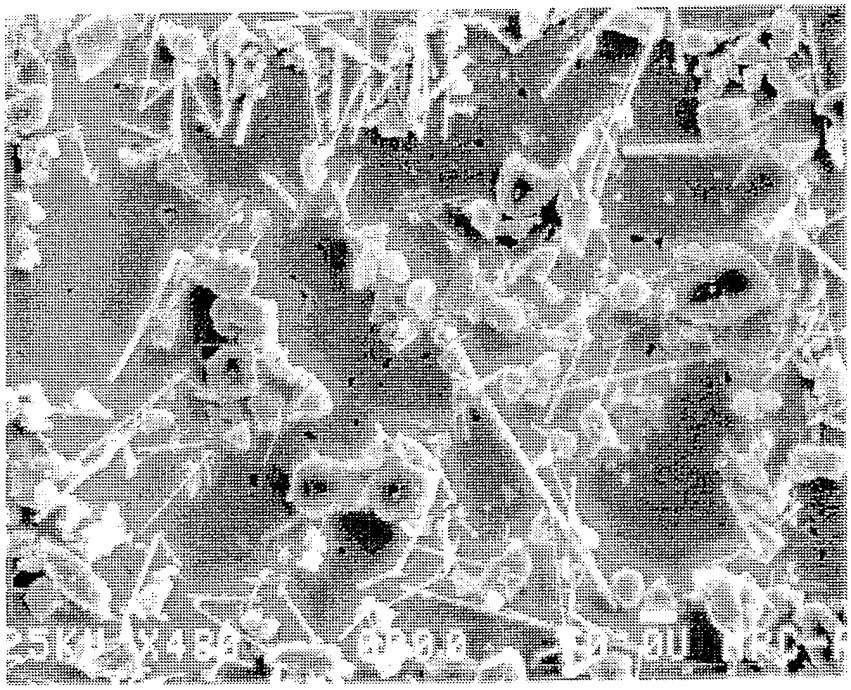

Figure 2. Scanning electron micrograph showing the relative sizes of particles and whiskers.

Table II. Tape casting compositions.

a) The composition used to make cordierite (MAS) tape.

	$\%volume_{(slurry)}$	$\%volume_{(green\ tape)}$
Stage I		
MAS	24	67
Toluene	25.7	-
Ethanol	38.5	-
Z-3	1.3	3.6
Stage II		
B-76	7.1	19.8
S-160	1.7	4.8
PEG-400	1.7	4.8

b) The composition used to make SiC_w reinforced tape (MAS+20$\%_{vol}$ SiC_w).

	$\%volume_{(slurry)}$	$\%volume_{(green\ tape)}$
Stage I		
MAS	16.4	54.6
SiC_w	4.1	13.7
Toluene	28.2	-
Ethanol	41.9	-
Z-3	1	3.2
Stage II		
B-76	5.6	19.3
S-160	1.4	4.6
PEG-400	1.4	4.6

Preparation of the tape casting slurry requires a two stage mixing process. In the first stage the ceramic frit powder (or frit+whiskers) were dispersed in solvent. The objective here is to separate each particle with the aid of a dispersing agent, Z-3, prior to the introduction of organic binders. Stage I consisted of low speed ball milling a 100 ml batch for 24 hours in a 250ml Nalgene bottle filled to ¼ of it's vertical depth with ⅜ inch zirconia media balls. Complete dispersion was verified by placing a few drops of the mixture on a slate slab and allowing them to dry. If no clumping of the powder is observed the mixture is thoroughly dispersed.

The binder, B-76, plasticizer, S160 and release agent, PEG 400, were added in the second stage. The stage II mixture was ball milled at low speed for 24 hours. Insignificant reduction of the particle size and whisker length resulted from mixing.

2. Casting. Prior to casting the tape the residual air trapped in the slurry must be removed. The mixture was poured into a plastic cup and placed into a vacuum chamber. The mixture frothed as the chamber was evacuated and collapsed as the vacuum was relieved. The frothing/collapsing sequence was repeated until a constant boiling of the mixture was observed, indicating all of the residual air had been removed. To remove any skin that may have formed during the de-airing procedure, the mixture was strained through a stainless steel screen into the doctor blade reservoir.

Casting was performed on plate glass with the aid of a doctor blade. A schematic of the doctor blade is depicted in Figure 3. The glass was prepared by thoroughly cleaning with detergent and waxing with PEG 400.

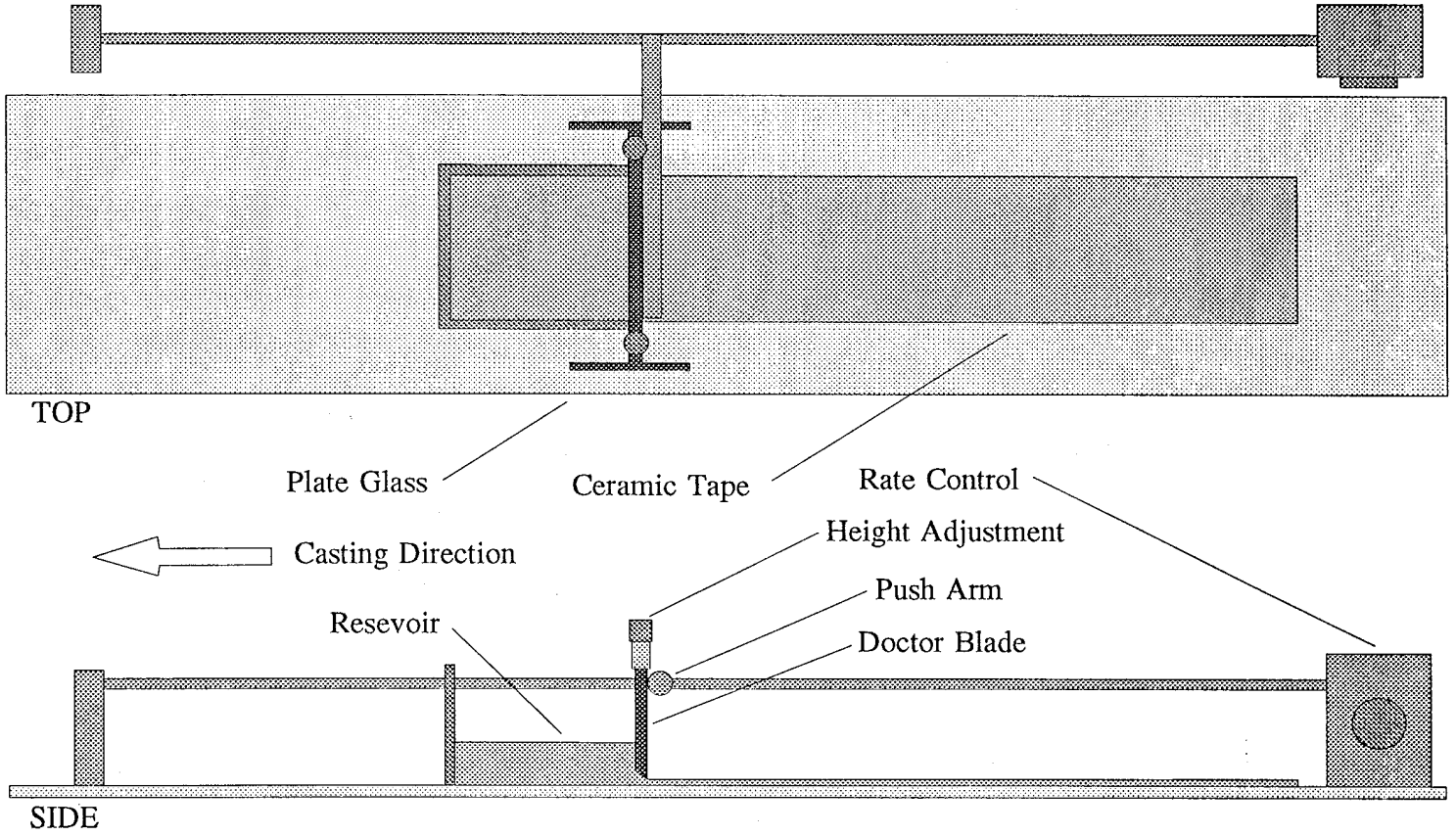

Figure 3. Schematic diagram of the tape casting apparatus.

The doctor blade controls the casting width and thickness as well as the casting rate. The least count of the blade height adjustment was 0.001 inch. Tapes were cast at 5 inch and 3 inch widths at a rate of 20 inches per minute to a length of about 35 inches. Tapes were dried in front of a ventilation hood to prevent the buildup of volatile fumes.

The casting thickness, t_o, is determined by the desired dense thickness, t. The dense thickness, fiber diameter, d, and fiber spacing, s, were used to define the target volume fractions of fiber and matrix in the composite. Assuming a uniform cross-section throughout the of the depth composite, cross-sectional areas were used to define the volume fraction of fiber, v_f, so that,

$$v_f = \frac{A_{fiber}}{A_{composite}} \tag{1}$$

where,

$$A_{fiber} = \pi \frac{d^2}{4}$$

$$A_{composite} = s\ t + A_{fiber}$$

The required fully dense matrix thickness can be found using the relation,

$$t = A_{fiber} \frac{v_f^{-1} - 1}{s} \tag{2}$$

The blade height for the proper casting thickness is given by[24],

$$t_o = \frac{t}{C_1 \cdot C_2 \cdot C_3} \tag{3}$$

where the constants of equation (3) represent,

C_1 - shrinkage during drying

C_2 - net amount of ceramic powder in the tape

C_3 - relative density of the burned out casting

The numerical value for C_1 is approximately equal to (1 - V_s), where V_s is the volume fraction of solvent in the slurry. The exact value for C_1 is unknown since 3-5 $\%_{vol}$ of the solvent will evaporate during the de-airing procedure and the combination of friction at the casting surface and gravity tend to cause the tape to shrink more in the vertical direction. C_2 is the shrinkage that results from burning out the organic materials and is nearly equal to powder loading in the tape. The final constant, C_3, is the shrinkage due to densification during hot press sintering. C_1 and the product C_2C_3 were experimentally determined for each formulation to provide uniform results.

The tapes required about 4 hours to dry completely. Removal consisted of loosening the edges with a razor blade and gently peeling the tape from the glass. Tapes were assigned a serial number and stored rolled in brown wrapping paper.

Some preferential alignment of whiskers during casting was expected and can be observed in the SEM images shown in Figure 4. The degree of alignment depends on casting thickness, casting rate, mixture viscosity and blade geometry[17]. Thinner tapes, higher casting rates, lower viscosity and rounded blade tips increase whisker alignment.

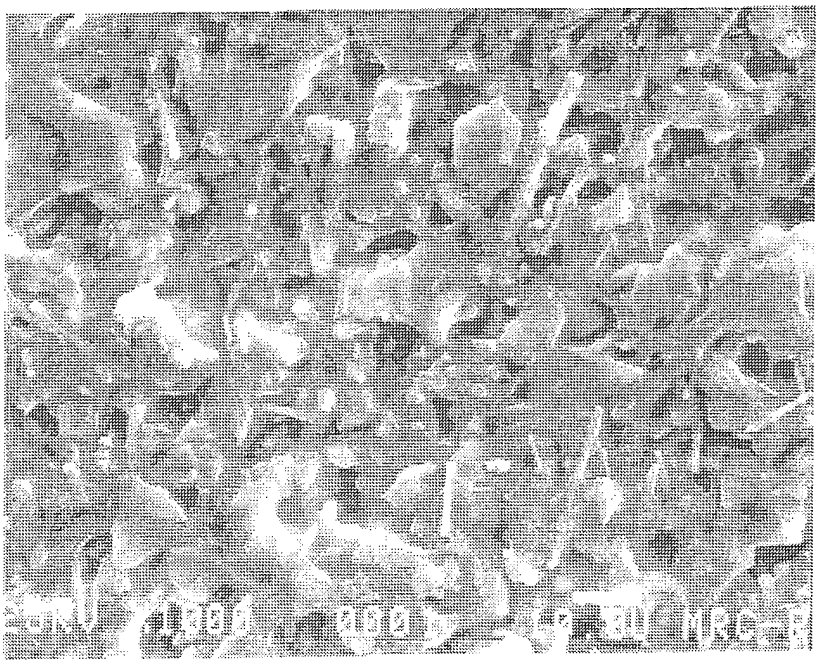

a) Upper (exposed) casting surface.

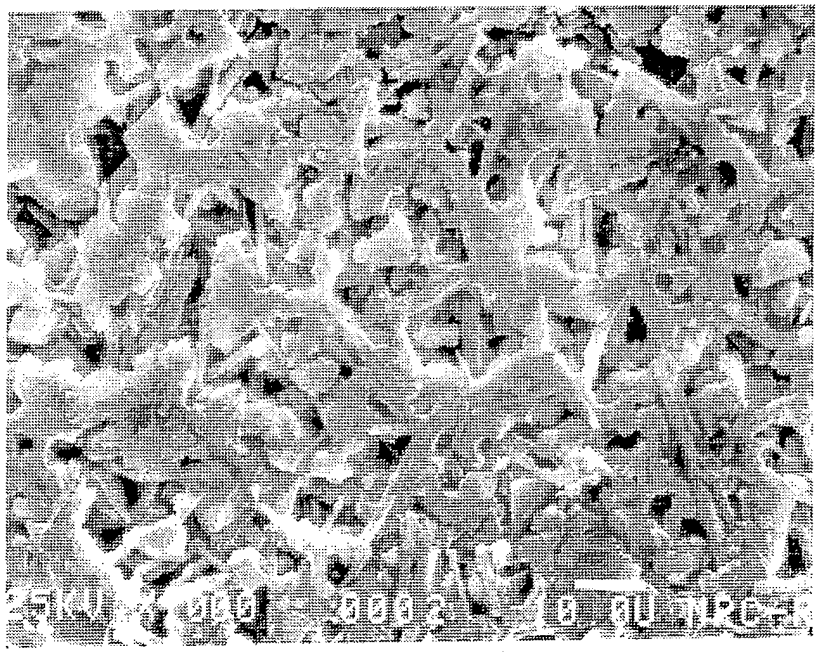

b) Lower (glass) casting surface.

Figure 4. Electron micrographs showing preferential alignment of whiskers in the MAS+20%$_{vol}$SiC$_w$ unfired tape.

B. LAMINATION

The construction of the specimen plates required three major steps. The fibers were first embedded into the ceramic tape. The fiber/tape laminae were then cut and indexed to provide the desired fiber packing, either hexagonal or cubic. The final step was to stack and laminate the plate in a graphite mold. The mold designed for the purpose of hot pressing a rectangular plate is shown in Figure 5.

1. Fiber Pre-impregnation. Sigma fibers are 102μm diameter fibers with SiC deposited on 20μm W cores and coated with TiB_2. The fiber mats received from the Atlantic Research Corporation consisted of Sigma fibers spaced at either 120 fibers/inch or 64 fibers/inch and adhered to heavy aluminum foil with polyvinyl alcohol. The mats measured either 10 inches wide (perpendicular to the fiber) by 24 inches long or 12 inches wide by 48 inches long.

Single layer prepregs were prepared by embedding Sigma fiber mat strips, cut in width to the fiber length dimension of the mold, into the ceramic tape strips. The single layer lay-ups were pressed at about 20 psi between platens heated to 80°C as shown in Figure 6. A symmetrical "sandwich" was used to facilitate the pressing of several layers simultaneously. The aluminum backing of the fiber mat was placed against the silicone rubber while the ceramic tape was placed against the silicone foam pad. Pressing in this fashion allows the tape to flex across the fibers, thus reducing spreading between fibers and preventing cutting of the tape.

To take advantage of the partial alignment of whiskers for enhancing transverse properties in the HCMC specimens, the tape strips were cut so that the casting direction would be perpendicular to the embedded fiber.

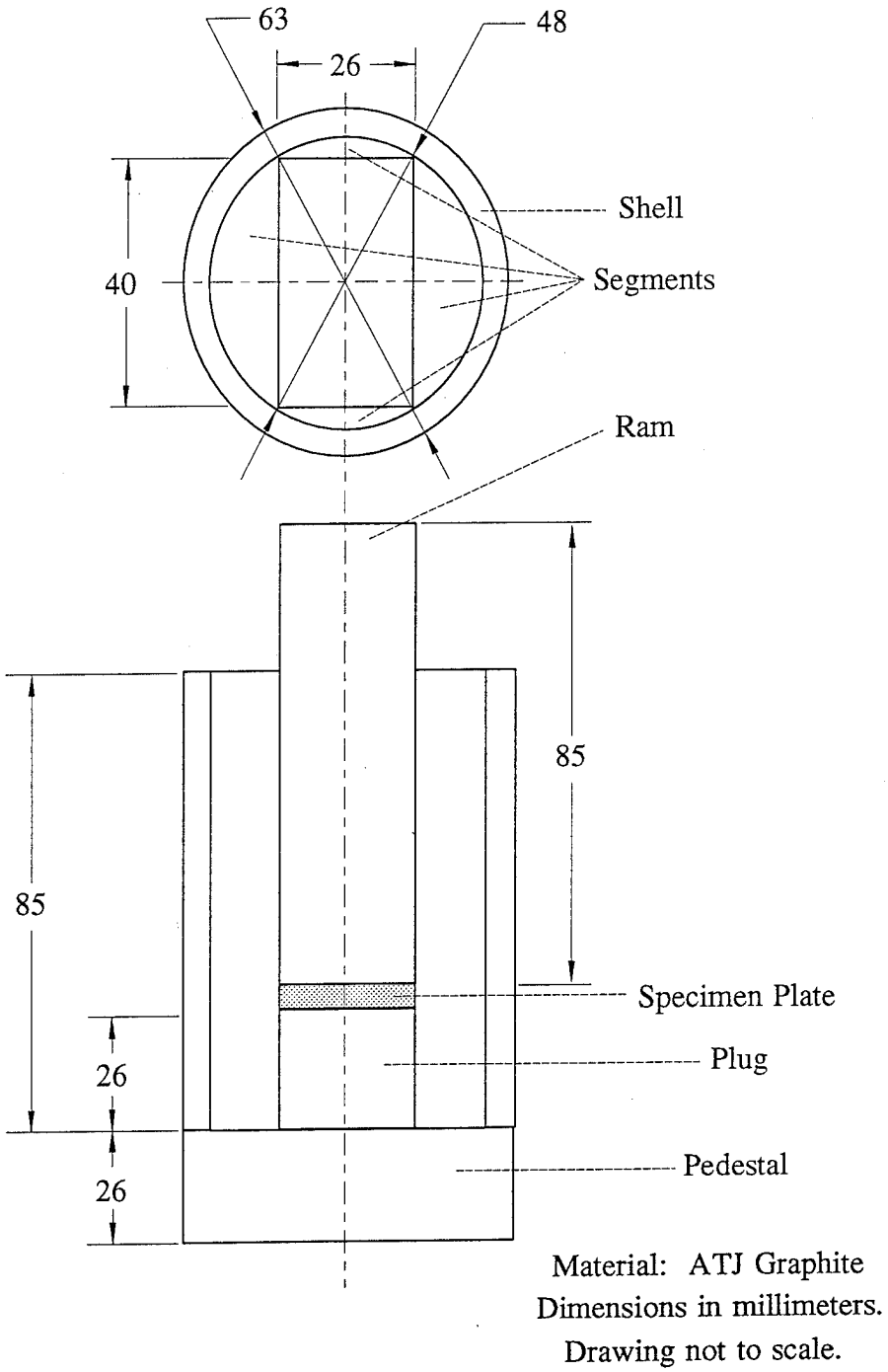

Figure 5. The graphite mold used to make rectangular plates in the hot press.

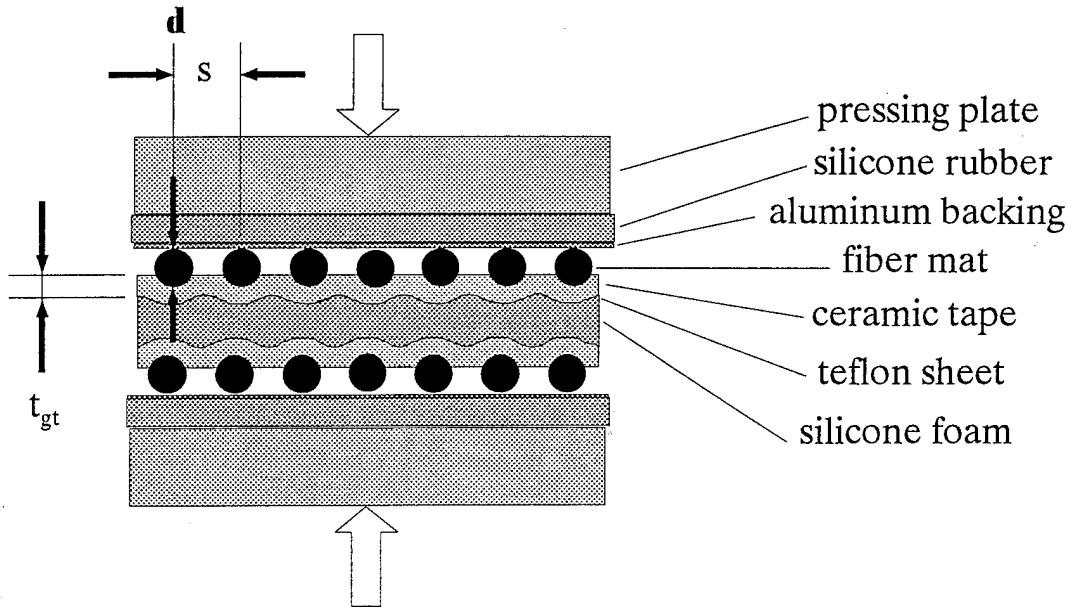

Figure 6. Lay-up for laminating two sets of pre-preg strips at the same time.

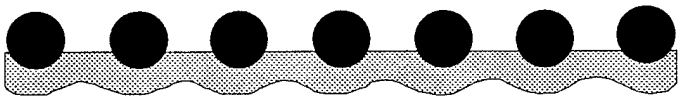

a) Fiber index edge layer.

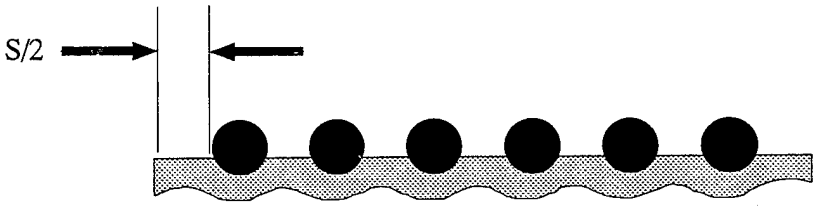

b) Offset index edge layer.

Figure 7. Preparation of the laminae indexing edges.

2. Indexing. The pre-preg laminae were first cut in length to the dimension of the mold perpendicular to the fiber direction. There are two different types of indexed edges as shown in Figure 7. The first type of index is made by cutting the tape, under stereo-microscope at a magnification of 16X, along the fiber. These are referred to as fiber index layers. Offset index layers were prepared by cutting the tape so as to leave an s/2 wide strip exposed beyond the first fiber.

3. Plate Lamination. To produce the desired final specimen thickness the appropriate number of layers required needed to be determined. The number of layers to use was found by dividing the intended plate thickness, t_{sp}, by the composite dense layer thickness, $t_c = A_{composite}/s$. For monolithic and whisker reinforced specimens, only neat matrix tape layers were used with the number of layers required based on the matrix dense layer thickness, t. For cubic packing, only fiber index layers were used. To provide hexagonal fiber packing, fiber index and offset index layers were alternately placed into the mold with the index edges against one side. A neat matrix tape layer was added to the top to complete the assembly. The stack was then lamination pressed in the mold at 80°C. The configuration for laminating the plate with hexagonal fiber packing can be seen in Figure 8.

C. THERMAL PROCESSES

Densification of the specimen plate required two distinct thermal processes. The organic constituents of the plate are first removed through a two step burnout procedure. The burned out casting was then moved to a hot press furnace where it was densified and heat treated.

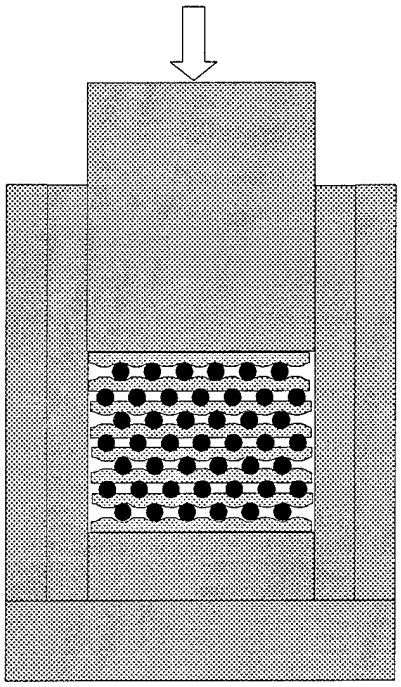

Figure 8. Lamination pressing the plate in the graphite mold.

1. Burnout

Prior to sintering, the organic materials needed to be removed from the laminated specimen plate. Thermolysis profiles from thermal gravimetric analysis (TGA) show that weight percent of B-76 drops rapidly at about 375°C and goes to zero by 575°C when

heated a rate of 10 C°/min[24]. Burnout was performed in an NEY model 2-525 dual rate/setpoint furnace. The green casting was heated to 90°C and soaked for 1 hour to remove moisture before heating to 500°C and burned out in air for 3 hrs. A heating rate of 1 C°/min was maintained to avoid delamination.

2. Hot Press and Heat Treat

A hot pressing and heat treating firing schedule was adapted from Ferro's suggested firing schedules for pressureless sintering of cordierite glass-ceramic frits[21]. Consideration was given to the condition of pressure assisted sintering that results in lower temperatures and higher rates for densification and crystallization. An Astro model HP20-3060-20 hot press furnace was used to perform the hot press and heat treat procedure. The temperature and pressure conditions used throughout the course of the process are presented graphically in figure 9.

The mold containing the burned out casting was heated in Argon to 900°C at a rate of 5 C°/min in a hot press furnace. After a 15 minute soak to assure uniform temperature inside the mold, the plate was slowly pressed to 1000 psi and continued to soak 15 minutes to densify. The pressure was then reduced to about 50psi to assure the pressing ram kept in contact with the mold during heat treatment. This was done so that the expected change in thickness due to the glass-to-crystal phase transformation could be observed.

The matrix material was fully crystallized by increasing the temperature to 1150°C at a rate of 2 C°/min and soaking for 2 hours. Following heat treatment, the cool down rate was maintained at 5 C°/min.

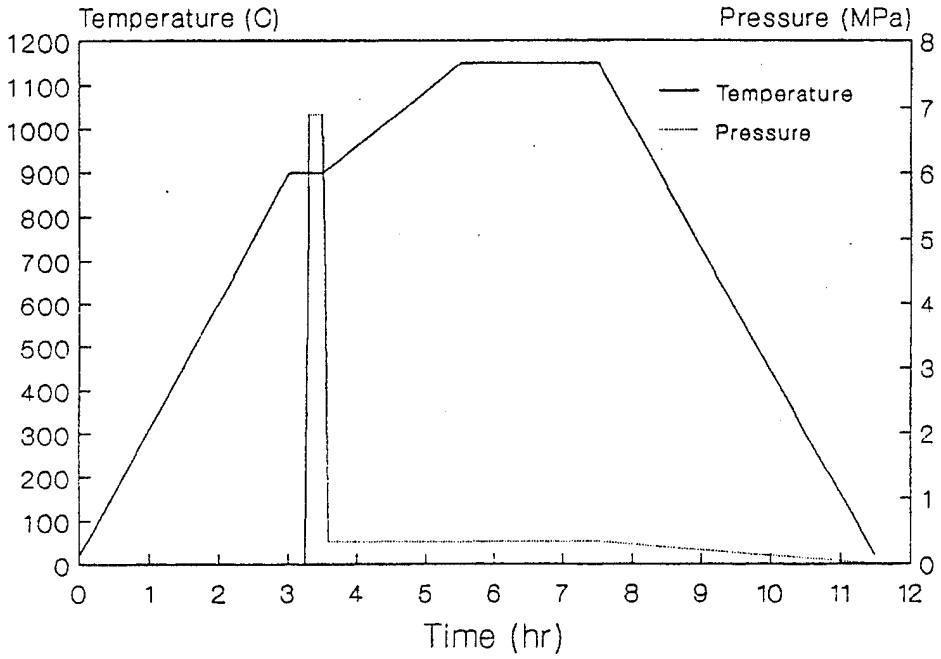

Figure 9. Hot pressing and heat treating variables as functions of time.

D. SPECIMEN PREPARATION

The specimen plates produced measured 40 mm X 26 mm X 3.25±0.25 mm. Grinding and polishing was performed on a two speed turntable with the method given in figure 10. A high quality surface polish is necessary for observing microcracks and to provide adequate acoustic coupling for the AE transducer.

The plates were cut into specimen bars for either axial or transverse mechanical characterization as shown in figure 11. Since, at the time of this study, there existed no standard for flexural testing of CMCs, the specimen dimensions for a flexural span of 35 mm were based on ASTM D-3552 for metal matrix composites[26].

1. Polishing The first step in specimen preparation was to surface grind the plate using a 15 micron diamond faceting disk. One end of the plate was also ground to reveal the fibers for subsequent volume fraction calculations. The faces and end of the plate were then polished to remove surface defects using 600 and 800 grit silicon carbide sand paper. Final polishing was made using 1 μm and 0.05 μm Al_2O_3 polishing powder on a flocked twill cloth. Water was used as a lubricant for grinding and polishing. The plate was carefully cleaned between each stage to avoid contamination of the previous grit size. Microscopic inspection of the surfaces was also made between each stage to assure all of the scratches from the previous stage had been removed. After the plate was completely dry it was measured and weighed for plate density calculations.

2 Cutting Each plate was cut into either five bars, measuring 40 mm X 4 mm X 3.25 ± 0.25 mm for axial specimens, or four bars, measuring 40 mm X 5 mm X 3.25 ± 0.25 mm for transverse specimens, at low speed using an Isomet diamond wafering saw. Cutting oil was removed from each specimen using acetone. The individual specimens were then repolished to remove edge defects that result from cutting. After thorough cleaning and microscopic inspection the specimens were marked with an identification number indicating the plate of origin and their location in the plate. Cross-sectional micrographs were taken from at least one specimen from each plate for volume fraction, porosity and fiber packing analysis. Finally, the density of each specimen was measured using Archimedes' principle.

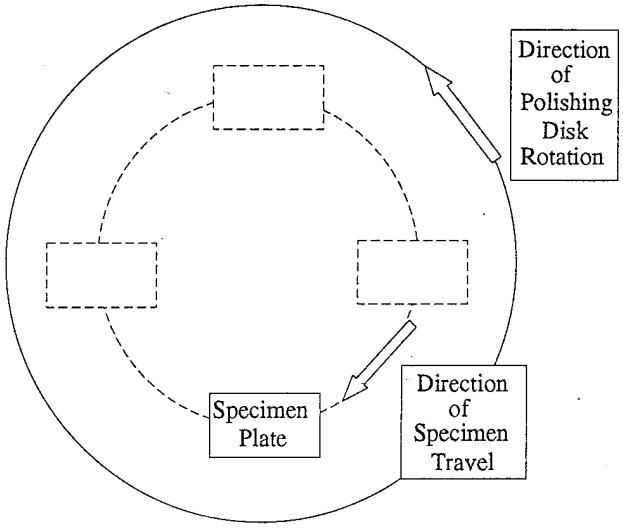

Figure 10. Method used for grinding and polishing.

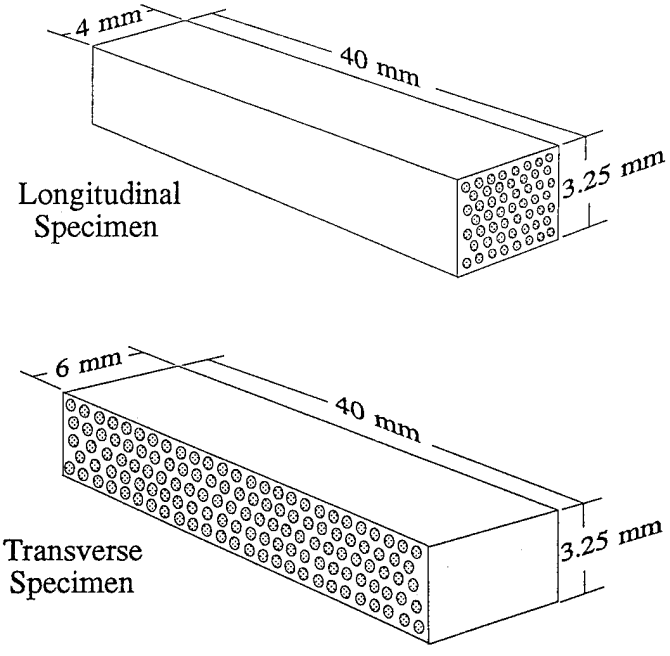

Figure 11. Dimensions for axial and transverse specimens.

IV. ANALYSIS

In the early stages of this study the constants C_1, C_2 and C_3 needed to be determined so that the casting thickness, t_o, produced the required dense thickness, t, within the matrix of the composite. Whisker reinforced tapes were examined to observe the extent of whisker degradation from ball mixing and the degree of whisker alignment that results from tape casting.

The initial step in specimen analysis was to determine the actual volume fractions of fibers, v_f', in the composites. The measured values of v_f' were then compared with the desired values, v_f, and subsequently used to find the theoretical composite densities. Values for bulk densities were measured and used along with the theoretical densities to calculate the specimen's porosity. Young's modulus, flexural strength and the microcracking stress were determined using 3-point bend testing with acoustic emission monitoring.

A. TAPE CASTING CONSTANTS

The shrinkage due to drying, C_1, is found by simply dividing the casting height, t_o, by the green tape thickness, t_{gt},

$$C_1 = \frac{t_{gt}}{t_o} \qquad (4)$$

Since the burned out casting is too fragile to remove from the mold to measure it's thickness, the product of C1· C2 was calculated using monolithic and WCMC specimen plates. With N_l as the number of layers and t_{sp} as the final dense plate

thickness,

$$C_1 \cdot C_2 = \frac{t_{sp}}{N_l \cdot t_{gt}} \qquad (5)$$

B. WHISKER ALIGNMENT

To determine the proportion of alignment , a vinyl overlay of the SEM image of the tape (see figure 4) was first used to mark all of the visible whiskers oriented $\pm 45°$ of the $0°$ direction. Another overlay was used to record the number of whiskers oriented $\pm 45°$ of the $90°$ direction. The percentage of alignment was then found by dividing the number of whiskers within a given orientation range by the total number of marked whiskers.

C. VOLUME FRACTIONS

There are two methods for finding the volume fraction of fibers in the composite. Both methods make use of backscattered electron images (BEI) of the specimen cross-sections as shown in figure 12. The cross-section is assumed to be uniform through the material to the extent of it's length. Enlarged copies of the micrographs were used to reduce the error associated with the precision of the measurements.

For regular fiber packing arrangements a unit cell can be defined by the average measured fiber horizontal spacing, s', and vertical spacing, t'. The fiber volume fraction is calculated with respect to the measured fiber diameter, d'.

$$v_f' = \frac{\pi (d')^2}{4\, s'\, t'} \qquad (6)$$

The second method of finding v_f' can be used for irregular fiber arrangements but more fibers are needed in the image to find the average value. The composite area is defined by the width, w, and height, h, of the field of view. After counting the number of fibers, N_f, the average fiber volume fraction in the composite is found using the measured fiber diameter, d′.

$$v_f' = \frac{N_f \, \pi \frac{(d')^2}{4}}{w \cdot l} \tag{7}$$

The volume fraction of whiskers in the matrix, v_w, is fixed at the time the mixture is prepared. The volume fraction of whiskers in the hybrid composite, v_w', depends on the value of v_f'.

$$v_w' = v_w \, (1 - v_f') \tag{8}$$

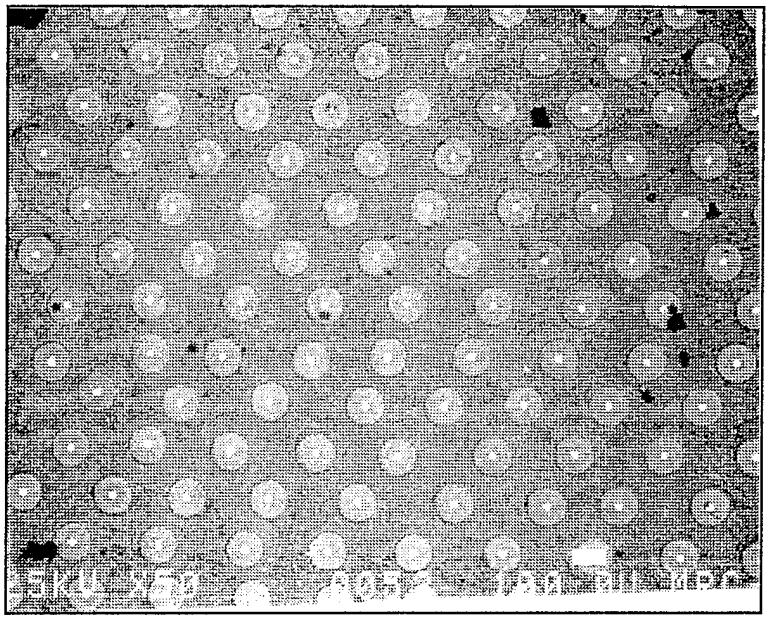

a) Continuous fiber specimen with composition MAS+30.1%$_{vol}$SiC$_f$.

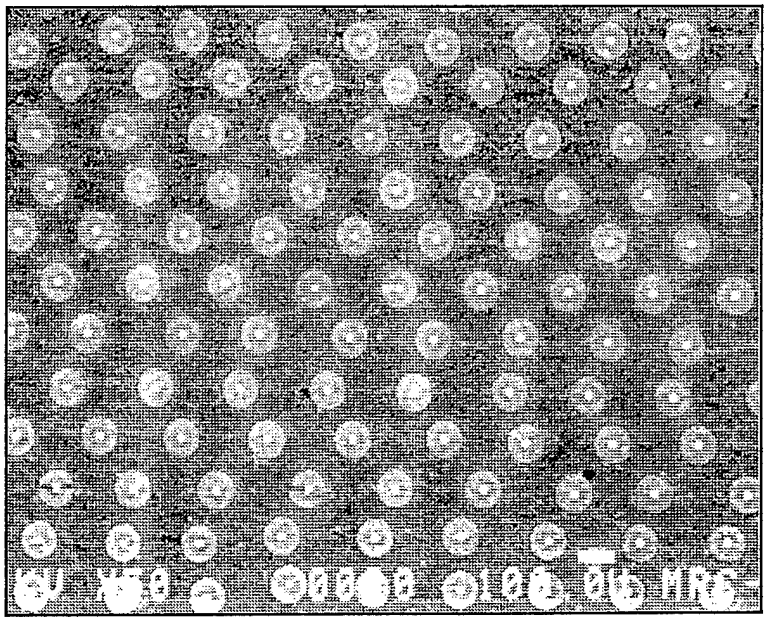

b) Hybrid specimen with composition MAS+24.8%$_{vol}$SiC$_f$+15.1%$_{vol}$SiC$_w$.

Figure 12. BEI electron micrographs of the composite cross-sections.

D. THEORETICAL DENSITY

For the monolithic specimens the theoretical density provided by the manufacturer was used[23]. Theoretical densities for the fibers and whiskers were found in "Ceramic Source"[28]. The rule of mixtures approach was used to find the theoretical density of the composite materials. With the subscript denoting either the component or composite density and using the volume fractions as previously defined gives,

$$\rho_{WCMC} = v_w \rho_{whisker} + (1 - v_w)\rho_{cordierite} \quad (9)$$

$$\rho_{FCMC} = v_f' \rho_{fiber} + (1 - v_f')\rho_{cordierite} \quad (10)$$

$$\rho_{HCMC} = v_f' \rho_{fiber} + v_w' \rho_{whisker} + (1 - v_f' - v_w')\rho_{cordierite} \quad (11)$$

E. BULK DENSITY

The bulk density, or mass per unit volume, was determined using Archimedes' principle[1]. The specimens were first weighed to find the dry weight, W_{dry}. The buoyant weight, $W_{buoyant}$, was measured with the specimen suspended in water. After lightly drying the visible surface moisture, the specimen was weighed once more to find the saturated weight, $W_{saturated}$. The bulk density could then be calculated using the equation,

$$\rho_{bluk} = \frac{W_{dry}}{W_{saturated} - W_{buoyant}} \quad (12)$$

F. POROSITY

The porosity of the fabricated composite can be found using the relative density[1]. The relative density is determined by the ratio of the measured bulk density to the calculated theoretical density. The volume fraction of pores in the specimen is then unity less the relative density. The percentage of porosity in the specimen is given by,

$$\% \text{ porosity} = \left(1 - \frac{\rho_{bulk}}{\rho_{theoretical}}\right) \text{ X } 100\% \qquad (13)$$

G. YOUNG'S MODULUS

Three point flexural testing was performed using an MTS model 810 servo-hydraulic system. Specimens were subjected to monotonic loading across a span of 35 mm. Data was collected using both PCLab data acquisition software running on an IBM PC XT and a mechanical plotter. The experimental setup is depicted in figure 13. Measurements consisted of applied load, P, and cross-head displacement, δ, which are used to calculate a measured stiffness, $K_m = P/\delta$.

The cross-head displacement that is measured for a given applied load results from both the compliance of the specimen, $1/K_{sp}$, and the compliance of the entire load frame system, $1/K_{sys}$. The measured compliance, $1/K_m = \delta/P$, can be modeled as the equivalent compliance of springs in series,

$$\frac{1}{K_m} = \frac{1}{K_{sp}} + \frac{1}{K_{sys}} \qquad (14)$$

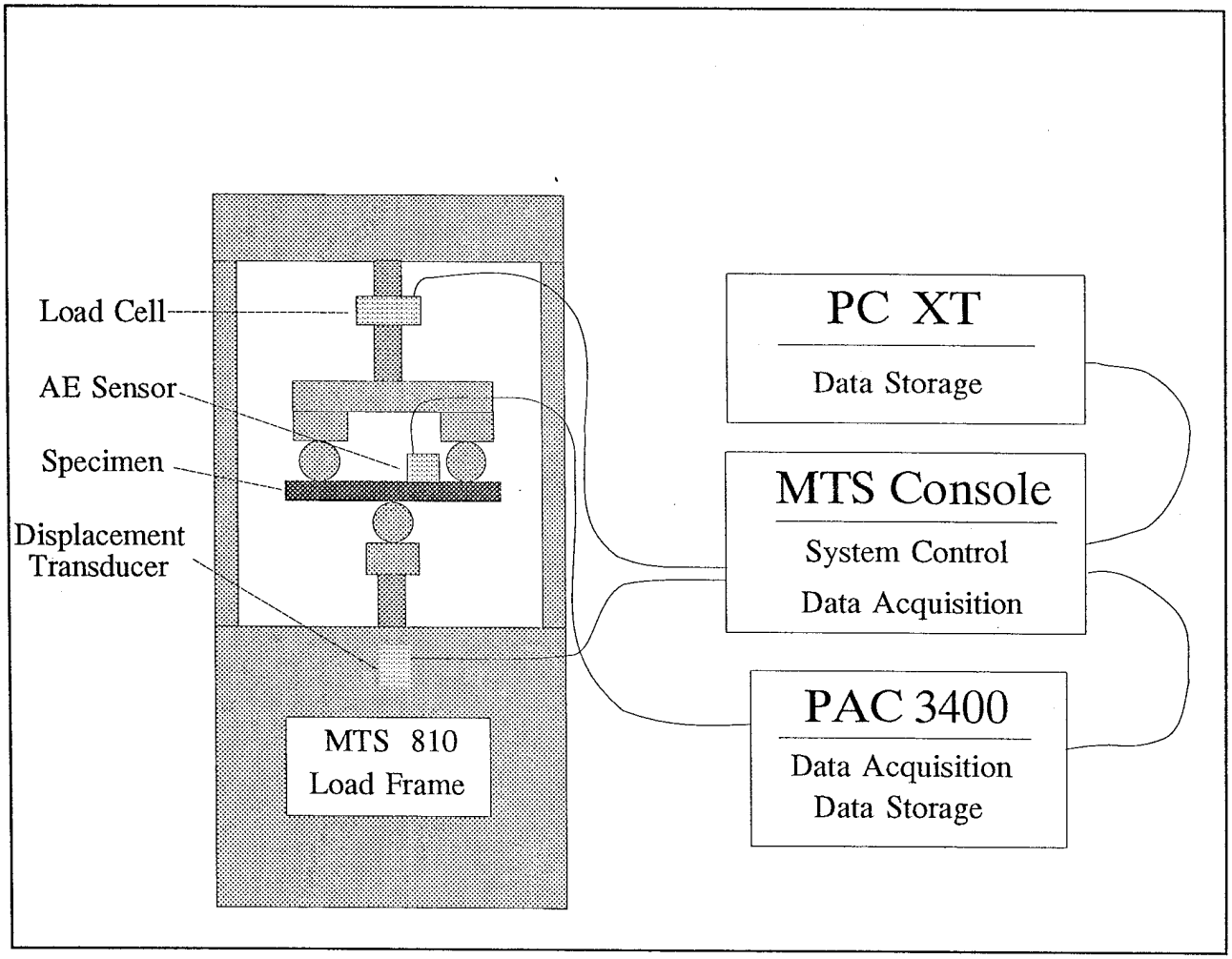

Figure 13. Experimental setup used for mechanical property characterization.

Evaluating the stiffness for a specimen of known elastic modulus, E, height, h, width, b, to be loaded across span, L, we have,

$$K_{sp} = \frac{48EI}{L^3} \tag{15}$$

where the area moment of inertia, I, is,

$$I = \frac{bh^3}{12} \tag{16}$$

The system compliance was found with equation (14) using data from a series of tests performed on the specimen of known stiffness. Young's modulus was then determined using,

$$E = \left(\frac{\delta}{P} - \frac{1}{K_{sys}}\right)^{-1} \frac{L^3}{48I} \tag{17}$$

H. STRESS AND STRAIN

Values used for the stress-strain curves were calculated from the load data contained in the PCLab output files. The maximum stress, σ_{max}, in a simply supported beam of rectangular cross-section loaded at the center is given by[27],

$$\sigma_{max} = \frac{Mc}{I} \tag{18}$$

with M=PL/4 and c=h/2.

The strain on the surface of the tension side of the beam is determined by[27],

$$\epsilon_{max} = \frac{\sigma_{max}}{E} \tag{19}$$

The stress associated with the onset of matrix microcracking was found via acoustic emission monitoring. A transducer from a Physical Acoustics Corporation model 3400 acoustic emission analyzer was attached to the specimen as shown in figure 13. Maximum sensitivity was limited by the level of noise in the system. The threshold and gain were adjusted so that the noise from the system was eliminated. The load at which emissions were observed was recorded and used in equation (18) to obtain the microcracking stress.

The proportional limit was found by inspecting the stress strain curve. Example plots from each type of material system are presented in figure 14. The stress at which the curve deviates from linearity defines the proportional limit. The flexural strength or modulus or rupture (MOR) was given by the maximum stress realized at the point of failure.

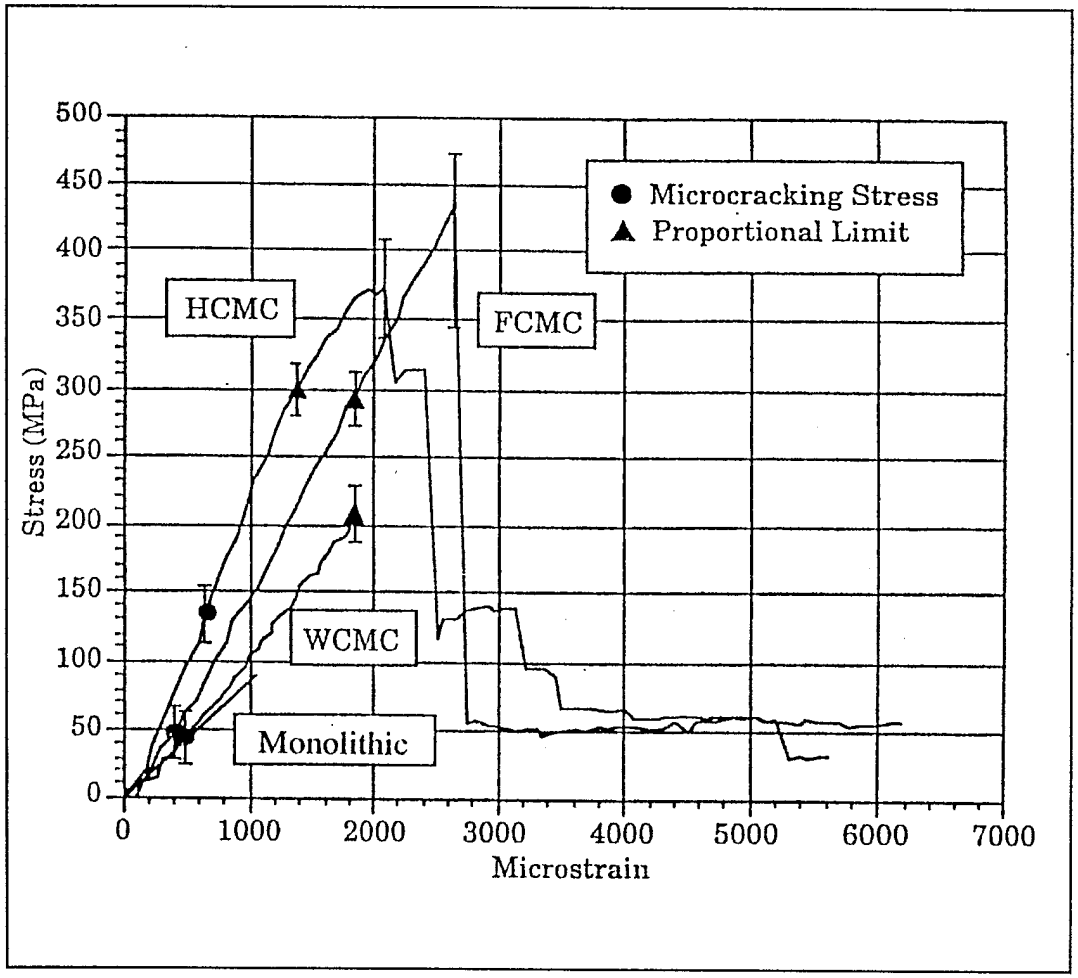

Figure 14. Typical stress-strain curves for monolithic (MAS), WCMC (MAS + 20%$_{vol}$ SiC_w), FCMC (MAS + 30%$_{vol}$ SiC_f) and HCMC (MAS + 25%$_{vol}$ SiC_f +15%$_{vol}$ SiC_w) specimens.

V. RESULTS

A. TAPE CASTING

The solvent based tape casting system used in this research yielded tapes that had very good strength and pliability. The unused tapes were examined after 18 months of storage and were found to have stiffened slightly but continued to be of sufficient quality to be useful. Green tape thicknesses were consistent and could be adjusted to within $\pm 12.7\mu m$ of the desired values. The experimentally determined casting constants for both formulations are given in table III.

Whiskers were observed to be partially aligned as opposed to completely random. The extent to which the whiskers were aligned through the thickness was not evaluated since cutting the tape would disturb their orientation. Electron micrographs of the upper and lower surfaces of a cordierite+20%$_{vol}$ whisker tape are shown in figure 4. Under the casting conditions used, an average of $67.6 \pm 2.9\%$ of the whiskers were aligned to within $\pm 45°$ of the casting direction at the surface of the tape.

Table III. Casting constants for the cordierite and cordierite+20%$_{vol}$ SiC_w formulations.

Composition	Casting Constants	
	C_1	$C_1 \cdot C_2$
MAS	0.393 ± 0.002	0.401 ± 0.008
MAS+20%$_{vol}$ SiC_w	0.483 ± 0.005	0.462 ± 0.017

B. SPECIMEN ATTRIBUTES

Specimens were fabricated with fairly uniform fiber spacing which approach the desired hexagonal packing arrangement as can be seen in figure 12. Fiber volume fractions could be controlled to within 1-2% of the target value. Measured fiber volume fractions can be compared with their intended values in table V. Theoretical densities of the components used to fabricate the composites are given in table IV. There was no detectectable porosity under SEM inspection. Table V also gives the average porosity calculated for each set of specimens.

The residue from grinding and polishing was examined with an electron microscope. There were no whiskers seen to be free from the matrix particles.

C. MECHANICAL PROPERTIES

The system stiffness, K_{sys}, was found to be 6778 ± 128 kN/m. The experimentally determined average values for Young's moduli (E_{11} and E_{22}), flexural strength and microcracking stress are presented in table VI. The axial stress-strain curves for typical specimens from one composition of each material system are shown in figure 14.

Toughening mechanisms associated with fiber and whisker pullout were obseved. Electron micrographs of fracture surfaces presented in figure 15 show both fiber and whisker pullout in an HCMC specimen.

Table IV. Properties of the constituents of the composites[22,28].

Constituent	Density (g/cm3)	Young's Modulus (GPa)	Flexural Strength (MPa)	Tensile Strength (MPa)
Cordierite	2.53	117	110	54
Sigma SiC_f	3.4	410	-	3450
SiC_w	3.2	580	-	8300

Table V. Target and average measured volume fractions along with average porosity.

Material System	Volume Fraction (%)				Porosity (%)
	Target		Measured		
	fiber	whisker	fiber	whisker	
Monolithic	0	0	-	-	0.08±0.03
WCMC	0	20	-	-	0.8±0.6
FCMC	15	0	15.8±0.2	0	0.48±0.03
	25	0	24.8±0.1	0	2.51±2.56
	30	0	30.2±1.0	0	3.51±2.48
HCMC	15	17	15.8±0.2	16.8±0.1	3.28±1.73
	25	15	25.8±1.1	14.8±0.3	7.14±3.07
	30	14	29.7±0.4	14.1±0.1	4.75±0.37
	35	13	34.2±0.4	13.2±0.1	3.28±1.02

Table VI. Summary of axial and transverse material properties.

Material System	Volume Fraction		E_{11} (GPa)	E_{22} (GPa)	First Microcracking Stress (MPa)	Proportional Limit (MPa)	Flexural Strength (MPa)
	SiC_f (%)	SiC_w (%)					
Monolithic	0	0	118±10	118±10	98±10	98±10	98±10
Axial							
WCMC	0	20	159±12	-	45.4±2.5	45.4±2.5	45.4±2.5
FCMC	30.2±1.0	0	167±20	-	47.3±8	290±30	380±45
HCMC	25.8±1.1	14.8±0.3	178±23	-	121.4±19	300±20	380±30
	29.7±0.4	14.1±0.1	212±24	-	-	420±30	473±40
Transverse							
FCMC	15.8±0.2	0	-	69.5±14	16.4±1	22.5±3	24.2±6
	24.8±0.1	0	-	7.4±2.1	3.9±0.6	3.9±0.6	3.9±0.6
HCMC	15.8±0.2	16.8±0.1	-	131±14	31.0±7	54±20	62.4±7
	34.2±0.4	13.2±0.1	-	75.4±3.0	34.5±6.4	53.8±10	53.8±10

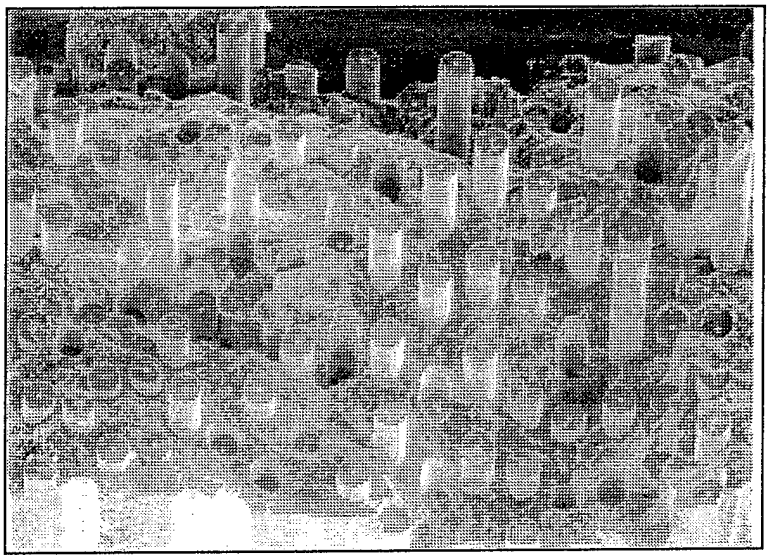

a) Fractograph showing fiber pullout.

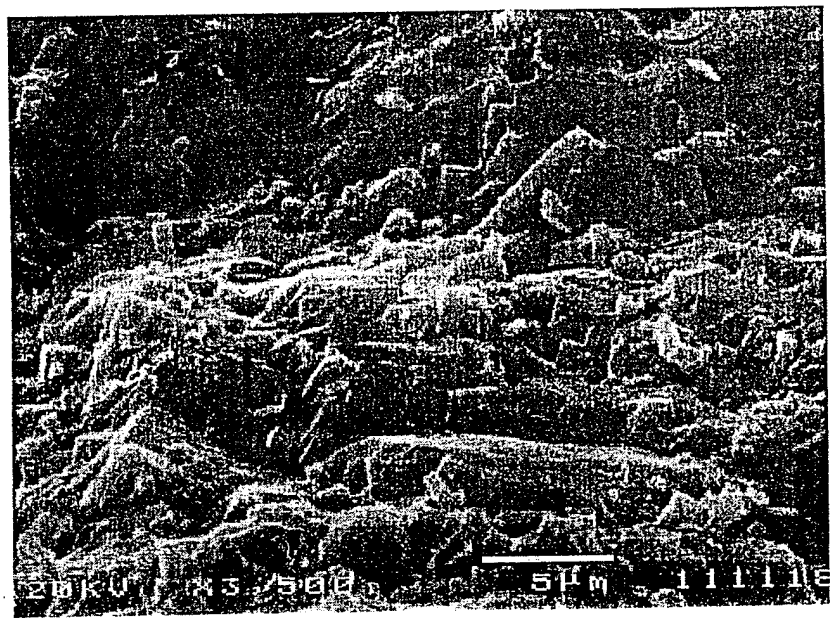

b) Close up view of the fracture surface exhibiting whisker pullout.

Figure 15. Fractographs of an HCMC specimen (SEI).

VI. CONCLUSION

The purpose of this study was to develop a technique by which uniform specimens could be fabricated consistently with specified constituent volume fractions. FCMC and HCMC plates consisting of $[0°]_{11s}$ and $[0°]_{12s}$ plys were produced to within ± 0.25 mm of the required specimen thickness. The fiber packing as seen from electron micrographs of typical cross-sections display fairly uniform, nearly hexagonal fiber distributions. On average, fiber volume fractions were produced to within $1 \pm 0.5\%_{vol}$ of the desired values. The highest average porosity was $7.14 \pm 3.07\%_{vol}$ but in most cases never exceeded $5\%_{vol}$. Tape casting and fiber lamination proved to be an exceptionally good method of fabricating ceramic matrix composites.

Although SiC whiskers require great care when handling prior to their introduction to the slurry mixture, they did not become free and friable as a result of grinding and polishing. This would indicate no extraordinary care is needed for post fabrication processes.

The HCMCs displayed improved stiffness, strength and damage tolerance capability when compared to the FCMCs of the same volume fraction of fibers. The effect of adding whiskers to the matrix of an FCMC was even more dramatic when the transverse characteristics are considered. The transverse stiffness, initial microcracking stress and flexural strength of the $15.8\%_{vol}$ SiC_f HCMC were approximately twice that of values found for the $15.8\%_{vol}$ SiC_f FCMC. Both fiber and whisker pullout were observed in HCMC specimens.

APPENDIX

SOURCES OF SUPPLY

Cordierite (MAS) (Glass/Ceramic Frit)	Ferro Corporation P. O. Box 6550 4150 East 56th Street Cleveland, OH 44101
Butvar® (B-76)	Monsanto Chemical Company 730 Worcester Street Springfield, Mass 01151
Santicizer® (S-160)	Monsanto Chemical Company 800 N. Lindbergh Blvd. St. Louis, MO 62167
Carbowax® (PEG-400)	Dow Chemical Midland, MI 48674
Defloc™ Z-3 (Blown Medhaden Fish Oil)	Werner G. Smith, Inc. 1730 Train Avenue Cleveland, OH 44113
Sigma (SiC_f) Fiber Mats	Atlantic Research Corp. 220 Ballard Vale Road Willmington, MS 01887
SiC Whiskers	Millennium Materials, Inc. 120 Sherlake Drive Knoxville, TN 37922
Graphite Mold	Graphite Products Corp. 1797 E. Ten Mile Road Madison Heights, MI 48071-4297

BIBLIOGRAPHY

1. D. W. Richerson, "Modern Ceramic Engineering : Properties, Processing, and Use in Design", 2nd ed., rev. and expanded, © 1992 by Marcel Dekker, Inc.

2. E. M. Logothetis, "ZrO_2 oxygen sensors in automotive applications", *Advances in Ceramics, Science and Technology of Zirconia*, American Ceramic Society, 3 388-405 (1981).

3. E. D. Whitney, "New Advances in Ceramic Tooling", *SME Tech. Rept. MRR75-15*, Society of Manufacturing Engineers, (1976).

4. L. J. Korb, *et al*, "The Shuttle Orbiter Thermal Protection System", *Bull. Amer. Ceram. Soc*, 60 [11] 1188-93 (1981).

5. R. N. Katz and J. G. Hannoosh, "Ceramics for High Performance Rolling Element Bearings", *Int. J. High Tech. Ceram.,* 1 [1] 68-79 (1985).

6. C. A. Fucinari and V. D. N. Rao, "Ceramic Regenerator Systems Development Program", *NASA CR-159707*, NASA contract DEN3-8, (1979).

7. H. E. Helms and F. A. Rockwood, "Heavy Duty Gas Turbine Engine Program", Progress Rept. July 1976 - Jan. 1978, *Rept. DDA EDR 9346*, NASA contract NAS3-20064, (1978).

8. K. M Johansen, *et al,*"Ceramic Components for Turbine Engines", 8th Interim Rept., *AiResearch Rept. 12-2794, 10*, Air Force contract F33615-77-C-5171, (1980).

9. H. R. Baumgartner, "Ceramic Bearings for Turbine Applications", *Ceramics for High Performance Applications*, pp. 423-43, © 1978 by Brook Hill.

10. "Making Ceramic Components for Advanced Aircraft Engines", *Nasa Tech. Briefs*, information packet LEW-15667 (1992).

11. A. G. Evans, "Perspective on the Development of High Toughness Ceramics", *J. Am. Ceram. Soc.* 73 [2] 187-206 (1990).

12. L. M. Sheppard, "Enhancing Performance of Ceramic Composites", *Am. Ceram. Bul.* 71 [4] 617-631 (1992).

13. K. T. Faber and A. G. Evans, "Crack Deflection Processes - I, Theory and II, Experiment", *Acta. Metall.*,31 [4] 565-84 (1983).

14. P. F Becher, et al., "Toughening Behavior in Whisker-Reinforced Ceramic Matrix Composites", *J. Am. Ceram. Soc.*, 71 [12] 1050-61 (1988).

15. S. R. Choi and J. A. Salem, "Strength, Toughness, and R-Curve Behavior of SiC Whisker Reinforced Silicon Nitride", *J. Mater. Sci., 27* [6] 1491-98 (1992).

16. H. Komada and T. Miyoshi, "Fabrication and Properties of Si_3N_4 Composites Reinforced by SiC Whiskers and Particles", *Ceram. Eng. Sci. Proc.,* 10 1072-82 (1989).

17. Claaßen, T., and Claussen, N., "Processing of Ceramic-Matrix/Platelet Composites by Tape Casting and Lamination", *J. Euro. Ceram. Soc.* 10 163-71 (1992).

18. L. A. Lewinsohn, "Hybrid Whisker-Fiber Reinforced Glass-Matrix Composites With Improved Transverse Toughness", *J. Mater. Sci. Let.,* 12 [18] 1478-1480 (1993)

19. L. R. Dharani, et al., "Microcracking Stress and Transverse Properties of Hybrid Ceramic Matrix Composites", *Ceram. Eng. Sci. Proc.*, 15 303-8 (1994).

20. E. Ryshkewitch and D. Richerson, "Oxide Ceramics", 2nd ed. p466, © 1985 by General Ceramics, Inc.

21. Dr. M. R. Reidmeyer's handout, "Formulations for Two Stage Organic Solvent Tape Casting Systems", University of Missouri - Rolla.

22. Personal correspondence from Dr. R. E. Dutton, U. S. Air Force Materials Laboratory, Dayton, Ohio.

23. Ferro's description pamphlet for MAS Glass/Ceramic Frit.

24. Birchall, J. D., et al, "Toxicity of Silicon Carbide Whiskers", *J. Mater. Sci. Let.*, 7 [4] 350-2 (1988)

25. Monsanto's description pamphlet for Butvar®.

26. ASTM D-3552-77, "Standard Test Method for Tensile Properties of Fiber-Reinforced Metal Matrix Composites", (1982).

27. A. Higdon, *et al*, "Mechanics of Materials", 4th ed, © by John Wiley & Sons, Inc. (1985).

28. "Ceramic Source", Vol. 8, © by American Ceramic Society, Inc. (1992).

VITA

Stephen Berry Haug was born in Kansas City, Missouri, on September 2, 1962. He also lived in Jefferson City, Missouri, and Belton, Missouri, before moving to Warrensburg, Missouri, in 1971. Mr Haug graduated from Warrensburg High School in 1980 and commenced his post secondary education at Central Missouri State University, also in Warrensburg. While attending CMSU, Mr. Haug worked as an outdoor power equipment technician for Lew's Engine Specialists, an instructional laboratory assistant for the Department of Chemistry and Physics and as a tutor for CMSU's Project Advance. Mr Haug was also supported by departmental Scholastic Achievement Awards from 1983 to 1985 and received the Outstanding Senior Student in Physics award before graduating CMSU, in May of 1985, with a Bachelor of Science degree in Physics.

Mr. Haug continued to work for Lew's, which had merged with a floral nursery to become Warrensburg Lawn and Garden Center, until he moved to Rolla, Missouri, in 1988 to pursue a degree in Aerospace Engineering at the University of Missouri-Rolla.

While attending UMR, Mr. Haug worked as an outdoor power equipment and tractor/trailer technician for Larry Davis Inc. in St. James, Missouri, from 1988 to 1993. He earned his Bachelor of Science degree in Aerospace Engineering in May of 1993, graduating cum laude. Mr. Haug remained at UMR to continue his education toward a Master of Science degree in Mechanical Engineering. He was supported as a Graduate Research Assistant through grants from the U. S. Air Force Office of Scientific Research and the Manufacturing Research and Training Center (Missouri Department of Economic Development).